OXFORD

Cerebral Cortex, 2023, **33**, 4939–4963
https://doi.org/10.1093/cercor/bhac391
Advance access publication date 13 October 2022
Original Article

Prefrontal and somatosensory-motor cortex effective connectivity in humans

Edmund T. Rolls [1,2,3,*], Gustavo Deco[4,5,6], Chu-Chung Huang[7,8], Jianfeng Feng[2,3]

[1]Oxford Centre for Computational Neuroscience, Oxford, UK,
[2]Department of Computer Science, University of Warwick, Coventry CV4 7AL, UK,
[3]Institute of Science and Technology for Brain Inspired Intelligence, Fudan University, Shanghai 200403, China,
[4]Computational Neuroscience Group, Department of Information and Communication Technologies, Center for Brain and Cognition, Universitat Pompeu Fabra, Roc Boronat 138, Barcelona 08018, Spain,
[5]Brain and Cognition, Pompeu Fabra University, Barcelona 08018, Spain,
[6]Institució Catalana de la Recerca i Estudis Avançats (ICREA), Universitat Pompeu Fabra, Passeig Lluís Companys 23, Barcelona 08010, Spain,
[7]Shanghai Key Laboratory of Brain Functional Genomics (Ministry of Education), Institute of Brain and Education Innovation, School of Psychology and Cognitive Science, East China Normal University, Shanghai 200602, China,
[8]Shanghai Center for Brain Science and Brain-Inspired Technology, Shanghai 200602, China

*Corresponding author: Department of Computer Science, University of Warwick, Coventry CV4 7AL, UK. Email: Edmund.Rolls@oxcns.org;
URL: https://www.oxcns.org

Effective connectivity, functional connectivity, and tractography were measured between 57 cortical frontal and somatosensory regions and the 360 cortical regions in the Human Connectome Project (HCP) multimodal parcellation atlas for 171 HCP participants. A ventral somatosensory stream connects from 3b and 3a via 1 and 2 and then via opercular and frontal opercular regions to the insula, which then connects to inferior parietal PF regions. This stream is implicated in "what"-related somatosensory processing of objects and of the body and in combining with visual inputs in PF. A dorsal "action" somatosensory stream connects from 3b and 3a via 1 and 2 to parietal area 5 and then 7. Inferior prefrontal regions have connectivity with the inferior temporal visual cortex and orbitofrontal cortex, are implicated in working memory for "what" processing streams, and provide connectivity to language systems, including 44, 45, 47l, TPOJ1, and superior temporal visual area. The dorsolateral prefrontal cortex regions that include area 46 have connectivity with parietal area 7 and somatosensory inferior parietal regions and are implicated in working memory for actions and planning. The dorsal prefrontal regions, including 8Ad and 8Av, have connectivity with visual regions of the inferior parietal cortex, including PGs and PGi, and are implicated in visual and auditory top-down attention.

Key words: prefrontal cortex; insula; somatosensory cortex; effective connectivity; human connectome.

Introduction

Given the great development and heterogeneity of functions of different parts of the human prefrontal as well as frontal cortex, and the importance of evidence about the connectivity of different cortical regions for understanding brain computations (Rolls 2000; Rajalingham et al. 2018; Zhuang et al. 2021; Rolls 2021c, 2021d), the aim of the present investigation is to advance the understanding of the connections and connectivity of the human prefrontal, frontal, and somatosensory cortical regions.

To do this, we measured with Human Connectome Project (HCP) data (Glasser, Smith, et al. 2016b) the direct connections between cortical regions using diffusion tractography; the functional connectivity (FC) between cortical regions using the correlation between the blood oxygen level–dependent (BOLD) signals in resting-state functional magnetic resonance imaging (rs-fMRI) which provides evidence about the strength of interactions; and the effective connectivity which provides evidence about the strength and direction of the causal connectivity between pairs of hundreds of cortical regions measured with a new Hopf algorithm (Rolls, Deco, et al., 2022b, 2022d, 2022e, 2022f). These measures were made between the 360 cortical regions in the HCP multimodal parcellation atlas (HCP-MMP) (Glasser, Coalson, et al. 2016a). The HCP-MMP atlas provides the most detailed parcellation of the human cortical areas that we know in that its 360 regions are defined using a multimodal combination of structural measures (cortical thickness and cortical myelin content), FC, and task-related fMRI (Glasser, Coalson, et al. 2016a). This parcellation is the parcellation of choice for the cerebral cortex because it is based on multimodal information (Glasser, Coalson, et al. 2016a) with the definitions and boundaries set out in their Glasser_2016_SuppNeuroanatomy.pdf, and it is being used as the basis for many new investigations of brain function and connectivity, which can all be cast in the same framework (Colclough et al. 2017; Van Essen and Glasser 2018; Sulpizio et al. 2020; Yokoyama et al. 2021; Rolls, Deco, et al. 2022b, 2022d, 2022e, 2022f; Rolls, Wirth, et al. 2022h). This approach provides better categorization of cortical areas than does, for example, FC alone (Power et al. 2011). A summary of the boundaries, tractography, FC, and task-related activations of frontal cortical areas using the HCP-MMP atlas is available elsewhere (Glasser, Coalson, et al. 2016a; Baker, Burks, Briggs, Conner, Glenn, Morgan, et al. 2018a; Baker, Burks, Briggs, Conner, Glenn, Robbins, et al. 2018b; Baker, Burks, Briggs, Conner, Glenn, Taylor, et al. 2018c; Baker, Burks, Briggs, Milton, et al. 2018d; Baker, Burks, Briggs, Sheets, et al. 2018e), but the effective connectivity, tractography, and FC analyses described here are new and are further presented in quantitative form using connectivity matrices for all 360 cortical areas.

Received: July 18, 2022. **Revised:** September 7, 2022. **Accepted:** September 8, 2022

As a background to help provide a framework for some of the connectivity described here, with the framework greatly developed in the Discussion, the following may be helpful as may be reference to Fig. 1. Area 3b is the primary somatosensory sensory cortex, with Area 3a, 1, and 2 also being important early somatosensory regions. The opercular regions are an inferior continuation of somatosensory processing areas that may be especially related to the face and head. In macaques, there are areas ventral to area 3b that include a second somatosensory region S2, and a parietal ventral area PV, but the correspondences with humans may be weak, with very little correspondence with rodents (O'Connor et al. 2021). Area 5 is a higher-order somatosensory processing region. In addition, there is a somatosensory hierarchy of cortical regions in the inferior parietal cortex somatosensory cortex progressing from PFcm and PFop to the top of the hierarchy in PF (Rolls, Deco, et al. 2022b). In macaques, PF is an inferior parietal cortex region primarily connected with somatosensory areas and with parietal and frontal face- and arm-related areas (Rozzi et al. 2006). The anterior ventral insular (AVI) area and the frontal opercular regions FOP3-5 ($y = \sim +26$ in Fig. S1-1) are where the human primary taste cortex is located in the anterior dorsal (i.e. superior) insula and adjoining frontal operculum (Rolls 2015, 2016a, 2016c). Area 7 of the parietal cortex, involved in visuomotor function, has connectivity directed to some intermediate stages of the somatosensory hierarchy (Rolls, Deco, et al. 2022b). The somatosensory system has an extensive connectivity with what is in a sense at least topologically a ventral extension of it, much of insular cortex. Area 4 is the primary motor cortex, and the areas 6 are premotor cortex, with much somatosensory processing directed toward these regions. The midcingulate cortex is a premotor area (Vogt 2016; Rolls, Wirth, et al. 2022h). In the inferior frontal gyrus, Broca's area 44 and 45 involved in language has connectivity not only with 47l and 55b but also with nearby inferior frontal IFJ and IFS regions (Rolls, Deco, et al. 2022d). The dorsolateral prefrontal cortex (DLPFC) regions are implicated in short-term memory (Funahashi et al. 1989; Goldman-Rakic 1996; Goldman-Rakic and Leung 2002) by maintaining firing in an attractor network (Martinez-Garcia et al. 2011; Fuster 2015; Constantinidis et al. 2018; Rolls 2021c). These prefrontal cortex regions are thereby involved in executive function (Fuster 2021; Passingham 2021) and top-down attention (Deco and Rolls 2004, 2005a, 2005b). The pregenual anterior cingulate cortex is activated by many rewards as is the medial orbitofrontal cortex (Grabenhorst and Rolls 2011; Rolls 2019b; Rolls et al. 2020), and the supracallosal anterior cingulate cortex is activated by many aversive subjectively unpleasant stimuli (Grabenhorst and Rolls 2011) but has connectivity with many somatosensory cortical regions as well as the pregenual anterior cingulate cortex and premotor regions (Rolls, Deco, et al. 2022f). It must be remembered that important inputs to at least the early somatosensory cortical regions and the taste cortex come from the thalamus (Delhaye et al. 2018).

The cortical regions included in this investigation can be thought of as including all of the frontal lobes apart from the orbitofrontal, ventromedial, and anterior cingulate cortex (which are considered elsewhere, Rolls, Deco, et al. 2022f). In addition, because the premotor and motor areas in the frontal cortex receive so extensively from postcentral somatosensory regions and the regions that receive from them, it is also very helpful to include these somatosensory regions in the present investigation. In addition, we note that the prefrontal cortex has connectivity with some premotor and somatosensory regions, as shown here, so it is helpful to include prefrontal cortex with the other cortical regions considered here.

The present research goes beyond this previous research by estimating causal, effective, connectivity between 57 frontal cortical regions in the human brain with a multimodal atlas with 360 cortical areas. Strengths of this investigation are that it utilized this HCP-MMP atlas (Glasser, Coalson, et al. 2016a); HCP data from the same set of 171 participants imaged at 7T (Glasser, Smith, et al. 2016b) in whom we could calculate the connections with diffusion tractography, FC, and effective connectivity; and that it utilized a method for effective connectivity measurement between all 360 cortical regions investigated here. The Hopf effective connectivity algorithm is important for helping to understand the operation of the computational systems in the brain, for it is calculated using time delays in the signals between 360 or more cortical regions (Rolls, Deco, et al., 2022b, 2022d, 2022e, 2022f), and the use of time is an important component in the approach to causality (Rolls 2021b). We hope that future research using the same brain atlas (Glasser, Coalson, et al. 2016a; Huang et al. 2022) will benefit from the human frontal cortical and related connectome described here.

Methods

Participants and data acquisition

Multiband 7T rs-fMRI of 184 individuals were obtained from the publicly available S1200 release (last updated: April 2018) of the HCP (Van Essen et al. 2013). Individual written informed content was obtained from each participant, and the scanning protocol was approved by the Institutional Review Board of Washington University in St. Louis, MO, United States (IRB #201204036).

Multimodal imaging was performed in a Siemens Magnetom 7T housed at the Center for Magnetic Resonance at the University of Minnesota in Minneapolis. For each participant, a total of 4 sessions of rs-fMRI were acquired, with oblique axial acquisitions alternated between phase encoding in a posterior-to-anterior (PA) direction in sessions 1 and 3, and an anterior-to-posterior (AP) phase encoding direction in sessions 2 and 4. Specifically, each rs-fMRI session was acquired using a multiband gradient-echo EPI imaging sequence. The following parameters were used: time repetition (TR) = 1,000 ms, time echo (TE) = 22.2 ms, flip angle = 45°, field of view = 208 × 208, matrix = 130 × 130, 85 slices, voxel size = 1.6 × 1.6 × 1.6 mm^3, and multiband factor = 5. The total scanning time for the rs-fMRI protocol was approximately 16 min with 900 volumes. Further details of the 7T rs-fMRI acquisition protocols are given in the HCP reference manual (https://humanconnectome.org/storage/app/media/documentation/s1200/HCP_S1200_Release_Reference_Manual.pdf).

The current investigation was designed to complement investigations of effective and FC and diffusion tractography of the hippocampus (Huang et al. 2021; Ma et al. 2022; Rolls, Deco, et al. 2022e); posterior cingulate cortex (Rolls, Wirth, et al. 2022h); parietal cortex (Rolls, Deco, et al. 2022b); orbitofrontal, ventromedial prefrontal, and anterior cingulate cortexes (Rolls, Deco, et al. 2022f); language cortical regions (Rolls, Deco, et al. 2022d); visual cortical regions (Rolls, Deco, et al. 2022a); and posterior parietal cortex regions (Rolls, Deco, et al. 2022b); and so, the same 171 participants with data for the rs-fMRI and diffusion tractography at 7T were used for the analyses described here (age: 22–36 years, 66 males).

Data preprocessing

The preprocessing was performed by the HCP as described in Glasser et al. (2013) based on the updated 7T data pipeline (v3.21.0,

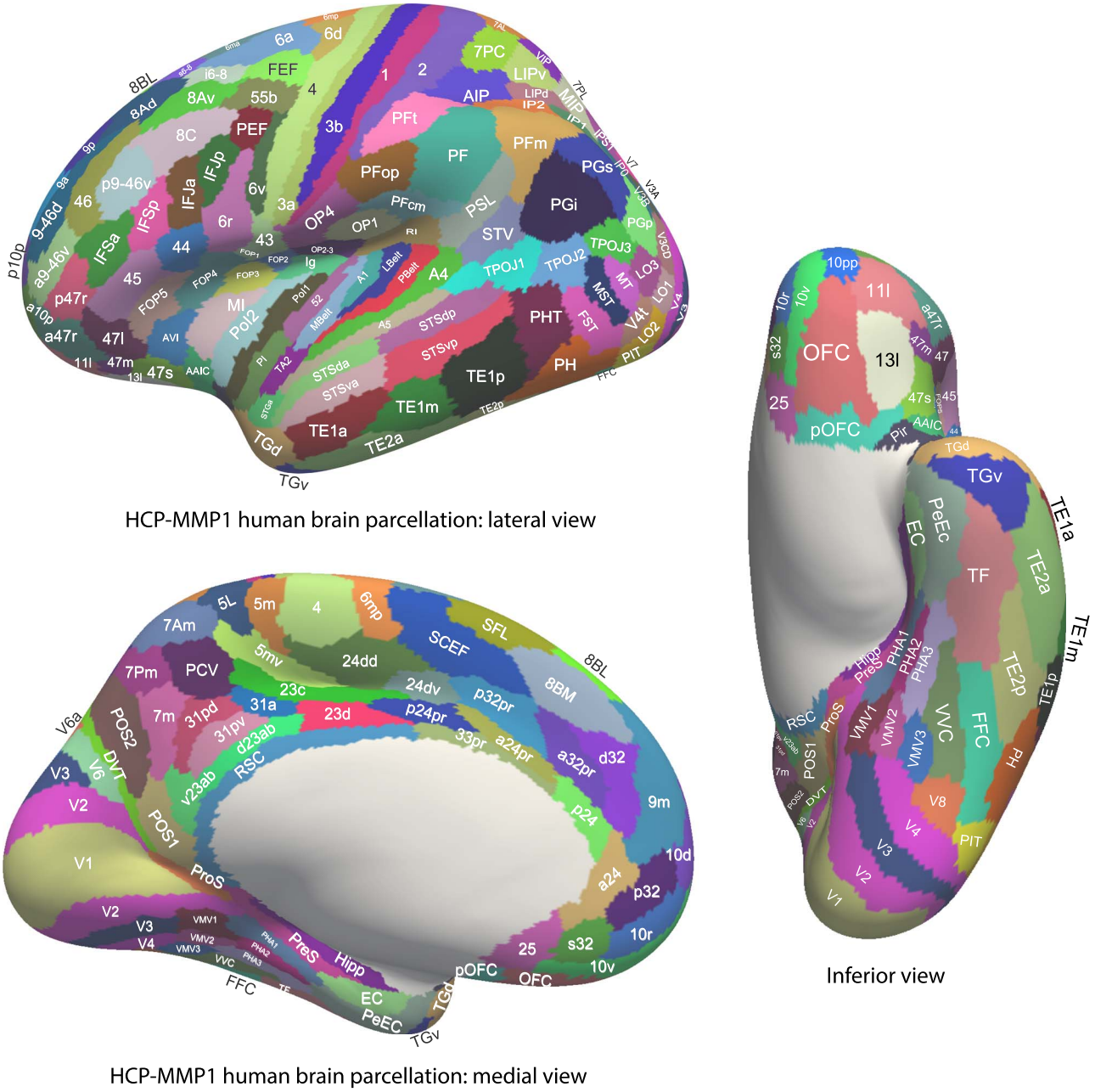

Fig. 1. Regions in the HCP-MMP (Glasser, Coalson, et al. 2016a) and its extended version HCPex (Huang et al. 2022) show the frontal cortex regions analyzed here. The regions are shown on images of the human brain, with the sulci expanded sufficiently to allow the regions within the sulci to be shown. Abbreviations are provided in Table S1. For comparison, a version of this diagram without the sulci expanded is provided in Fig. S1-5.

https://github.com/Washington-University/HCPpipelines), including gradient distortion correction, head motion correction, image distortion correction, and spatial transformation to the Montreal Neurological Institute space using 1-step spline resampling from the original functional images followed by intensity normalization. In addition, the HCP took an approach using ICA (FSL's MELODIC) combined with a more automated component classifier referred to as FIX (FMRIB's ICA-based X-noisifier) to remove nonneural spatiotemporal artifact (Smith et al. 2013; Griffanti et al. 2014; Salimi-Khorshidi et al. 2014). This step also used 24 confound timeseries derived from the motion estimation (6 rigid-body parameter timeseries, their backward-looking temporal derivatives, plus all 12 resulting regressors squared (Satterthwaite et al. 2013) to minimize noise in the data. The preprocessing performed by the HCP also included boundary-based registration between EPI and T1w images and brain masking based on FreeSurfer segmentation. The "minimally preprocessed" rsfMRI data provided by the HCP 1200 release (rfMRI*hp2000_clean.dtseries) was used in this investigation. The preprocessed data are in the HCP grayordinates standard space and are made available in a surface-based CIFTI file for each participant. With the MATLAB script (cifti toolbox: https://github.com/Washington-University/cifti-matlab), we extracted and averaged the cleaned timeseries of all the grayordinates in each region of the HCP-MMP 1.0 atlas (Glasser, Coalson, et al. 2016a), which is a group-based parcellation defined in the HCP grayordinate standard space having 180 cortical regions per hemisphere and is a surface-based atlas provided in the CIFTI

format. The timeseries were detrended and temporally filtered with a second-order Butterworth filter set to 0.008–0.08 Hz.

Brain atlas and region selection

To construct the effective connectivity for the regions of interest in this investigation with other parts of the human brain, we utilized the 7T rs-fMRI data the HCP and parcellated this with the surface based HCP-MMP atlas which has 360 cortical regions (Glasser, Coalson, et al. 2016a). We were able to use the same 171 participants for whom we also had performed diffusion tractography, as described in detail (Huang et al. 2021). The brain regions in this atlas (Glasser, Coalson, et al. 2016a) are shown in Fig. 1 and Fig. S1, and a list of the cortical regions in this atlas and the divisions into which they are placed is provided in Table S1 in the reordered form used in the extended volumetric HCPex atlas (Huang et al. 2022).

The 57 frontal and related cortical regions selected for connectivity analysis here were as follows, in the HCP-MMP division indicated (and set out in Table S1) where relevant. The strategy was to select in principle all cortical regions in the divisions of the MMP/HCPex atlas (see Table S1) that included the frontal cortex or were closely related to them. The divisions in the HCP-MMP/HCPex atlas (see Table S1) are: SomatoSensory-Motor, ParaCentral and MidCingulate, Premotor, Posterior Opercular, Insula-Frontal Opercular, IFG—Inferior Frontal Gyrus, and DLPFC—Dorsolateral Prefrontal Cortex. These divisions are separated by red lines in most of the figures, except that an extra red line was included with the IFG division to show Broca's area 44 and 45, and related orbital parts 47l and a47r, somewhat separated (by the red line) from the other inferior frontal gyrus regions. The only brain regions within these divisions that we did not include in the analyses described here and in the figures are the pyriform (olfactory) cortex, as that is not primarily somatosensory/motor or prefrontal, and the eye fields (FEF, PEF, and SCEF), as they are concerned with visual functions and have been included in an analysis of the connectivity of visual cortical areas (Rolls, Deco, et al. 2022a). The connectivity of the orbitofrontal cortex and anterior cingulate cortex is described elsewhere (Rolls, Deco, et al. 2022f). Background on the boundaries and activations found in each of the brain regions considered here is provided elsewhere (Glasser, Coalson, et al. 2016a; Baker, Burks, Briggs, Conner, Glenn, Morgan, et al. 2018a; Baker, Burks, Briggs, Conner, Glenn, Robbins, et al. 2018b; Baker, Burks, Briggs, Sheets, et al. 2018e).

It is noted that the HCP-MMP atlas sometimes uses dorsal versus ventral as descriptors following nomenclature in nonhuman primates and that these correspond to superior and inferior in humans. For those becoming familiar with the HCP-MMP atlas, in the name of a cortical region, typically a = anterior, p = posterior, d = dorsal (i.e. superior in the human brain), v = ventral (i.e. inferior in the human brain), m = medial, l or L = lateral, T = temporal, P = parietal, and V = visual. It must also be noted that some of the names used in the HCP-MMP atlas utilize the name of the corresponding region in macaques, but in humans, the cortical region may not be topologically in the same place (e.g. sulcus) as in macaques.

Measurement of effective connectivity

Effective connectivity measures the effect of one brain region on another and utilizes differences detected at different times in the signals in each connected pair of brain regions to infer effects of one brain region on another. One such approach is dynamic causal modeling, but it applies most easily to activation studies and is typically limited to measuring the effective connectivity between just a few brain areas (Friston 2009; Valdes-Sosa et al. 2011; Bajaj et al. 2016), though there have been moves to extend it to resting-state studies and more brain areas (Frassle et al. 2017; Razi et al. 2017). The method used here (see Rolls, Deco, et al. 2022e, 2022f) was developed from a Hopf algorithm to enable the measurement of effective connectivity between many brain areas, as described by Deco et al. (2019). A principle is that the FC is measured at time t and time $t+$ tau, where tau is typically 2 s to take into account the time within which a change in the BOLD signal can occur and that tau should be short to capture causality and then the effective connectivity model is trained by error correction until it can generate the FC matrices at time t and time $t+$ tau. Further details of the algorithm, and the development that enabled it to measure the effective connectivity in each direction, are described next and in more detail in the Supplementary Material.

To infer the effective connectivity, we use a whole-brain model that allows us to simulate the BOLD activity across all brain regions and time. We use the so-called Hopf computational model, which integrates the dynamics of Stuart-Landau oscillators, expressing the activity of each brain region by the underlying anatomical connectivity (Deco, Kringelbach, et al. 2017b). As mentioned above, we include in the model 360 cortical brain areas (Huang et al. 2022). The local dynamics of each brain area (node) is given by Stuart-Landau oscillators, which express the normal form of a supercritical Hopf bifurcation, describing the transition from noisy to oscillatory dynamics (Kuznetsov 2013). During the last years, numerous studies were able to show how the Hopf whole-brain model successfully simulates empirical electrophysiology (Freyer et al. 2011; Freyer et al. 2012), magnetoencephalography (Deco, Cabral, et al. 2017a), and fMRI (Kringelbach et al. 2015; Deco, Kringelbach, et al. 2017b; Kringelbach and Deco 2020).

The Hopf whole-brain model can be expressed mathematically as follows:

$$\frac{dx_i}{dt} = \overbrace{\left[a_i - x_i^2 - y_i^2\right]x_i - \omega_i y_i}^{\text{Local Dynamics}} + \overbrace{G\sum_{j=1}^{N} C_{ij}\left(x_j - x_i\right)}^{\text{Coupling}} + \overbrace{\beta\eta_i(t)}^{\text{Gaussian Noise}}, \quad (1)$$

$$\frac{dy_i}{dt} = \left[a_i - x_i^2 - y_i^2\right]y_i + \omega_i x_i + G\sum_{j=1}^{N} C_{ij}\left(y_j - y_i\right) + \beta\eta_i(t). \quad (2)$$

Equations (1) and (2) describe the coupling of Stuart-Landau oscillators through an effective connectivity matrix C. The $x_i(t)$ term represents the simulated BOLD signal data of brain area i. The values of $y_i(t)$ are relevant to the dynamics of the system but are not part of the information read out from the system. In these equations, $\eta_i(t)$ provides additive Gaussian noise with standard deviation β. The Stuart-Landau oscillators for each brain area i express a Hopf normal form that has a supercritical bifurcation at $a_i = 0$ so that, if $a_i > 0$, the system has a stable limit cycle with frequency $f_i = \omega_i/2\pi$ (where ω_i is the angular velocity); and when $a_i < 0$, the system has a stable fixed point representing a low activity noisy state. The intrinsic frequency f_i of each Stuart-Landau oscillator corresponding to a brain area is in the 0.008–0.08 Hz band ($i = 1, \ldots, 360$). The intrinsic frequencies are fitted from the data, as given by the averaged peak frequency of the narrowband BOLD signals of each brain region. The coupling term representing the input received in node i from every other node j is weighted by the corresponding effective connectivity C_{ij}. The coupling is the canonical diffusive coupling, which approximates the simplest (linear) part of a general coupling function. G denotes the global coupling weight, scaling equally the total input received

in each brain area. While the oscillators are weakly coupled, the periodic orbit of the uncoupled oscillators is preserved. Details are provided in the Supplementary Material.

The effective connectivity matrix is derived by optimizing the conductivity of each existing anatomical connection as specified by the Structural Connectivity matrix (measured with tractography, Huang et al. 2021) in order to fit the empirical FC pairs and the lagged FC^{tau} pairs. By this, we are able to infer a nonsymmetric effective connectivity matrix (see Gilson et al. (2016)). Note that FC^{tau}, i.e. the lagged FC between pairs, lagged at tau s, breaks the symmetry, and thus is fundamental for our purpose. Specifically, we compute the distance between the model FC simulated from the current estimate of the effective connectivity and the empirical data FC^{emp} as well as the simulated model FC^{tau} and empirical data FC^{tau_emp} and adjust each effective connection (entry in the effective connectivity matrix) separately with a gradient-descent approach. The model is run repeatedly with the updated effective connectivity until the fit converges toward a stable value.

We start with the anatomical connectivity obtained with probabilistic tractography from dMRI (or from an initial zero C matrix as described in the Supplementary Material) and use the following procedure to update each entry C_{ij} in the effective connectivity matrix

$$C_{ij} = C_{ij} + \varepsilon \left(FC_{ij}^{emp} - FC_{ij} + FC_{ij}^{tau\_emp} - FC_{ij}^{tau} \right), \quad (3)$$

where ϵ is a learning rate constant, and i and j are the nodes. When updating each connection if the initial matrix is a dMRI structural connection matrix (see Supplementary Material), the corresponding link to the same brain regions in the opposite hemisphere is also updated, as contralateral connections are not revealed well by dMRI. The convergence of the algorithm is illustrated by Rolls, Deco, et al. (2022e), and the utility of the algorithm was validated as described below.

For the implementation, we set tau to be 2 s, selecting the appropriate number of TRs to achieve this. The maximum effective connectivity was set to a value of 0.2 and was found between V1L and V1R.

Effective connectome

Whole-brain effective connectivity analysis was performed between the 57 frontal and related cortical regions described above (see Fig. 1 and Fig. S1) and the 360 regions defined in the surface-based HCP-MMP atlas (Glasser, Coalson, et al. 2016a) in their reordered form provided in Table S1, described in the Supplementary Material, and used in the volumetric extended HCPex atlas (Huang et al. 2022). This effective connectivity was computed for all 171 participants. The effective connectivity algorithm was run until it had reached the maximal value for the correspondence between the simulated and empirical FC matrices at time t and $t+$ tau (see Supplementary Material). The effective connectivity calculated was checked and validated in a number of ways described in the Supplementary Material and elsewhere (Rolls, Deco, et al. 2022a). The present algorithm was developed from an earlier approach that was extensively tested and validated (Gilson et al. 2016).

To test whether the vectors of effective connectivities of each of the 57 frontal and related cortex regions with the 180 areas in the left hemisphere of the modified HCP atlas were significantly different, the interaction term was calculated for each pair of the 57 cortex regions effective connectivity vectors in separate 2-way ANOVAs (each 2 × 180) across the 171 participants, and Bonferroni correction for multiple comparisons was applied. The results were checked with the nonparametric Scheirer-Rey-Hare test (Scheirer et al. 1976; Sinha 2022).

Functional connectivity

The FCs (Fig. 5) which represent a linear measure of connectivity (calculated with the Pearson correlation) range from close to 1.0 to −0.33, and with a threshold of 0.4, reveal somewhat more links than the effective connectivity, partly perhaps because they can reflect common input to 2 regions rather than causal connectivity between regions, and partly because the threshold has been set to reveal effects known in the literature but not reflected in the effective connectivity. The FCs are useful as a check on the effective connectivities but of course do not measure causal effects.

For comparison with the effective connectivity, the FC was also measured at 7T with the identical set of participants, data, and filtering of 0.008–0.08 Hz. The FC was measured by the Pearson correlation between the BOLD signal timeseries for each pair of brain regions and is in fact the FC^{emp} referred to above. A threshold of 0.4 is used for the presentation of the findings in Fig. 5, for this sets the sparseness of what is shown to a level commensurate with the effective connectivity, to facilitate comparison between the functional and the effective connectivity. The FC can provide evidence that may relate to interactions between brain regions, while providing no evidence about the causal direction-specific effects. A high FC may in this scenario thus reflect the strong physiological interactions between areas and provides a different type of evidence to effective connectivity. The effective connectivity is nonlinearly related to the FC, with effective connectivities being identified (i.e. >0) only for the links with relatively high FC.

The FC is shown in Fig. 5 and the diffusion tractography is shown in Fig. 6 for comparison with the effective connectivity. FC and diffusion tractography have been used in many previous investigations of the human connectome (Catani and Thiebaut de Schotten 2008; Glasser, Coalson, et al. 2016a; Maier-Hein et al. 2017) and therefore the comparison with effective connectivity is of interest.

Connections shown with diffusion tractography

Diffusion tractography can provide evidence about fiber pathways linking different brain regions with a method that is completely different to the ways in which effective and FC are measured, so it is included here to provide complementary and supporting evidence to the effective connectivity. Diffusion tractography shows only direct connections, so comparison with effective connectivity can help to suggest which effective connectivities may be mediated directly or indirectly. Diffusion tractography does not provide evidence about the direction of connections. Diffusion tractography was performed on the same 171 HCP participants imaged at 7T with methods described in detail elsewhere (Huang et al. 2021). The major parameters were: 1.05 mm isotropic voxels; a 2-shell acquisition scheme with b-values = 1,000, 2,000 s/mm^2, TR/TE = 7,000/71 ms, 65 unique diffusion gradient directions, and 6 b0 images obtained for each phase encoding direction pair (AP and PA pairs). Preprocessing steps included distortion correction, eddy-current correction, motion correction, and gradient nonlinearity correction. In brief, whole brain tractography was reconstructed for each subject in native space. To improve the tractography termination accuracy in GM, MRtrix3's 5ttgen command was used to generate multitissue segment images (5tt) using T1 images, and the segmented tissues were then coregistered with

the b0 image in diffusion space. For multishell data, the tissue response functions in GM, WM, and CSF were estimated by the MRtrix3' dwi2response function with the Dhollander algorithm (Dhollander et al. 2016). A MultiShell MultiTissue Constrained Spherical Deconvolution model with lmax = 8 and prior coregistered 5tt image was used on the preprocessed multishell DWI data to obtain the fiber orientation distribution (FOD) function (Smith 2002; Jeurissen et al. 2014). Based on the voxel-wise FOD, anatomically constrained tractography using the probabilistic tracking algorithm: iFOD2 (second-order integration based on FOD) with dynamic seeding was applied to generate the initial tractogram (1 million streamlines with maximum tract length = 250 mm and minimal tract length = 5 mm). To quantify the number of streamlines connecting pairs of regions, the updated version of the spherical-deconvolution informed filtering of the tractograms method was applied, which provides more biologically meaningful estimates of the structural connection density (Smith et al. 2015).

The results for the tractography are shown in Fig. 6 as the number of streamlines between areas with a threshold applied of 10 to reduce the risk of occasional noise-related observations. The highest level in the color bar was set to 1,000 streamlines between a pair of cortical regions in order to show graded values for a number of links, but the value for the number of streamlines between V1 and V2 was in fact higher at close to 10,000. The term "connections" is used when referring to what is shown with diffusion tractography and connectivity when referring to effective or FC.

The diffusion tractography (Fig. 6) provides no evidence on the direction or causality of connections and is useful as it can provide some evidence on what in the effective connectivity may reflect a direct connection and what does not. However, limitations of the diffusion tractography are that it cannot follow streamlines within the gray matter where the fibers become unmyelinated so the exact site of termination is not perfectly provided; and the tractography does not follow long connections well with, for example, almost none of the contralateral connectivity shown with tractography that is revealed by the effective connectivity in Figs. S2 and S3; and may thus overemphasize the connections between close cortical regions. Nevertheless, the diffusion tractography is a useful complement to the effective connectivity, especially where it provides evidence where an effective connectivity link may be mediated by a direct connection. On the other hand, the effective connectivity and FC are useful complements to the tractography by helping to exclude false positives in the tract-following in the tractography, as had been examined for the human hippocampal connectome (Huang et al. 2021; Ma et al. 2022; Rolls, Deco, et al. 2022e).

Results

Overview: effective connectivity, FC, and diffusion tractography

The effective connectivity to the 57 frontal and related cortical regions from other cortical regions in the left hemisphere are shown in Fig. 2. The effective connectivities from the 57 frontal cortical regions to other cortical regions in the left hemisphere are shown in Fig. 3. The vectors of effective connectivities of each of the 57 frontal cortical regions with the 180 regions in the left hemisphere of the HCP-MMP atlas were all significantly different from each other. (Across the 171 participants, the interaction term in separate 2-way ANOVAs for the comparisons between the effective connectivity of every pair of the 57 ROIs after Bonferroni correction for multiple comparisons were all $P < 10^{-90}$. The results were confirmed with the nonparametric Scheirer-Rey-Hare test; Scheirer et al. 1976; Sinha 2022.) The connectivity of each of the cortical divisions set out above are considered division by division in the Results, as this helps closely related regions to be described together and provides a useful framework. For all divisions, the text assumes reference to the data in Figs. 2–4. The effective connectivities described in the text are the stronger ones, typically >0.01, but all of those >0 are shown in the figures. In addition to the effective connectivity, the FC (Fig. 5) and diffusion tractography (Fig. 6) available for each cortical region are referred to where useful. The functional implications of the results described next are considered in the Discussion using Figs. 7–11 which may be helpful to view when the Results are considered.

Somatosensory/motor division (regions 1, 2, 3a, 3b, and 4)

Region **3b**, sometimes considered the primary somatosensory cortex, has very strong bidirectional effective connectivity (EC) with 3a (0.14), slightly stronger effective connectivity to region 1 (0.12) than from it (0.10), weaker effective connectivity with 2 (0.03), and stronger effective connectivity to 4 (primary motor cortex) (0.12) than from it (0.10) (Figs. 2 and 3). It also has moderate effective connectivity (0.03–0.05) with other somatosensory regions, including posterior opercular regions OP1-4, 5L, and 5m, and the insular granular complex region (Ig), and RetroInsular cortex RI. Region 3b also has effective connectivity with premotor regions 6mp and 6d and with midcingulate motor regions 24dd and 24dv. Hints of auditory effective connectivity are marginal.

Region **3a** has similar effective connectivity to 3b but in addition has some weak effective connectivity from auditory A1 and LBelt and marginal from V2 and V6 (Figs. 2 and 3).

Region **1** has stronger effective connectivity from 3b (0.12) than to it (0.10), and similarly for 3a (0.08 vs. 0.07), and there is strong effective connectivity from region 2 (0.11). Region 1 also receives more strongly from OP1-4 and from 5L and 5m and from Ig than it connects to them. Region 1 also has moderate connectivity to motor 4, premotor 6d, and midcingulate 24dd. There is also some effective connectivity from the MT and V4t regions in the MT+ complex in which responses are found to moving visual stimuli.

Region **2** has some connectivity with 3a and 3b (~0.03) but has strong connectivity with region 1 (0.11) and has moderate connectivity with 5L, OP1, and FOP2 (~0.06). Interestingly, there is strong effective connectivity from superior parietal regions (7AL, 7PC) (0.09) and with inferior parietal PFt (0.04). Effective connectivity is directed to premotor regions 6d, 6mp, and 6v and the midcingulate cortex. The other connectivities shown in Figs. 2 and 3 are <0.01.

These analyses are consistent with some hierarchical somatosensory organization from 3b (and 3a) to 1 and then to 2. There is connectivity of these regions with opercular regions and with parts of area 5.

Region **4**, the primary motor cortex, receives effective connectivity ranked as follows from 3a, 3b, 1, 24dd, 5m and 5L, 6mp, 6d, OP2-4, and the insula (Ig and RI).

Figure 4 emphasizes that midcingulate 24dv, and 5L, and OP2-4 have stronger connectivity toward 3a, 3b, 1, and 2 than from them. Figure 5 shows some FC of the regions in this division with some early visual cortical areas and dorsal visual and some MT+ regions, and with some auditory cortex regions, but the

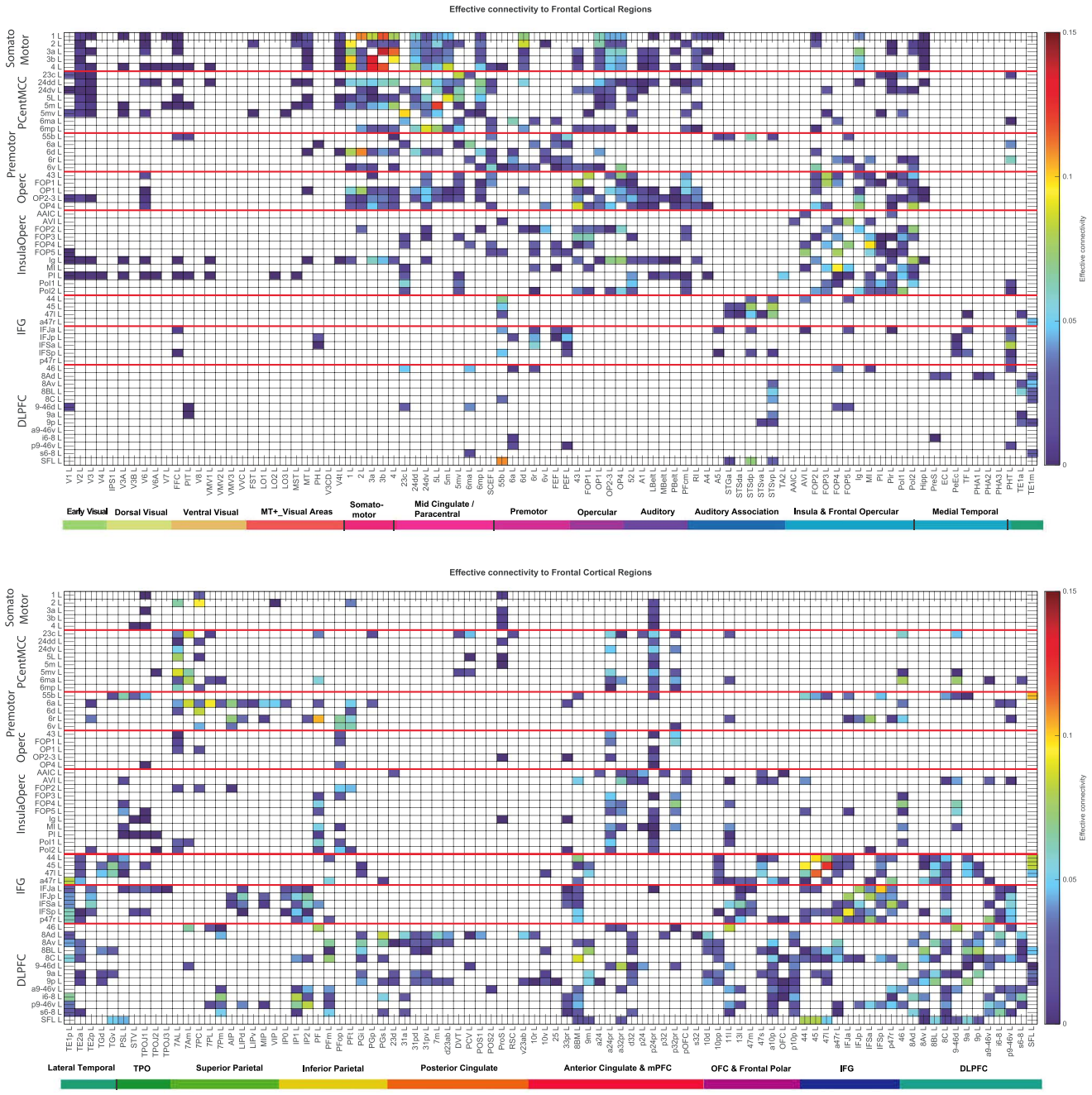

Fig. 2. Effective connectivity "TO" frontal cortical regions (the rows) "FROM" 180 cortical areas (the columns) in the left hemisphere. The effective connectivity is read from column to row. effective connectivities of 0 are shown as blank. All effective connectivity maps are scaled to show 0.15 as the maximum, as this is the highest effective connectivity found between this set of brain regions. The effective connectivity algorithm for the whole brain is set to have a maximum of 0.2, and this was for connectivity between V1 and V2. The effective connectivity for the first set of cortical regions is shown in the top panel; and for the second set of regions is shown in the lower panel. Abbreviations: see Table S1. The divisions in the HCP-MMP/HCPex atlas (see Table S1) are separated by red lines: SomatoSensory-Motor, ParaCentral and MidCingulate, Premotor, Posterior Opercular, Insula-FOP, IFG (which has an extra red lines to show Broca's area 44 and 45, and related orbital parts 47l and a47r from the other inferior frontal gyrus regions), and DLPFC. The colored labeled bars show the cortical divisions in the HCP-MMP atlas (Glasser, Coalson, et al. 2016a). The order of the cortical regions is that in Huang et al. (2022).

effective connectivity as shown in Figs. 2 and 3 is low. There is also some FC evident in Fig. 5 with the superior temporal visual area (STV) and TPOJ1-2, which together are parts of the language regions (Rolls, Deco, et al. 2022d), and with supracallosal parts of the anterior cingulate cortex p24pr and p32pr (which have FC with many regions in the somatosensory-motor, paracentral and MCC, premotor, opercular, and insular-opercular divisions, emphasizing the connectivity of the supracallosal anterior cingulate cortex with somatosensory-motor cortical regions; Rolls, Deco, et al. 2022f). The diffusion connectivity (Fig. 6) does not reveal direct connections of this somatosensory-motor division with visual cortical regions apart from the

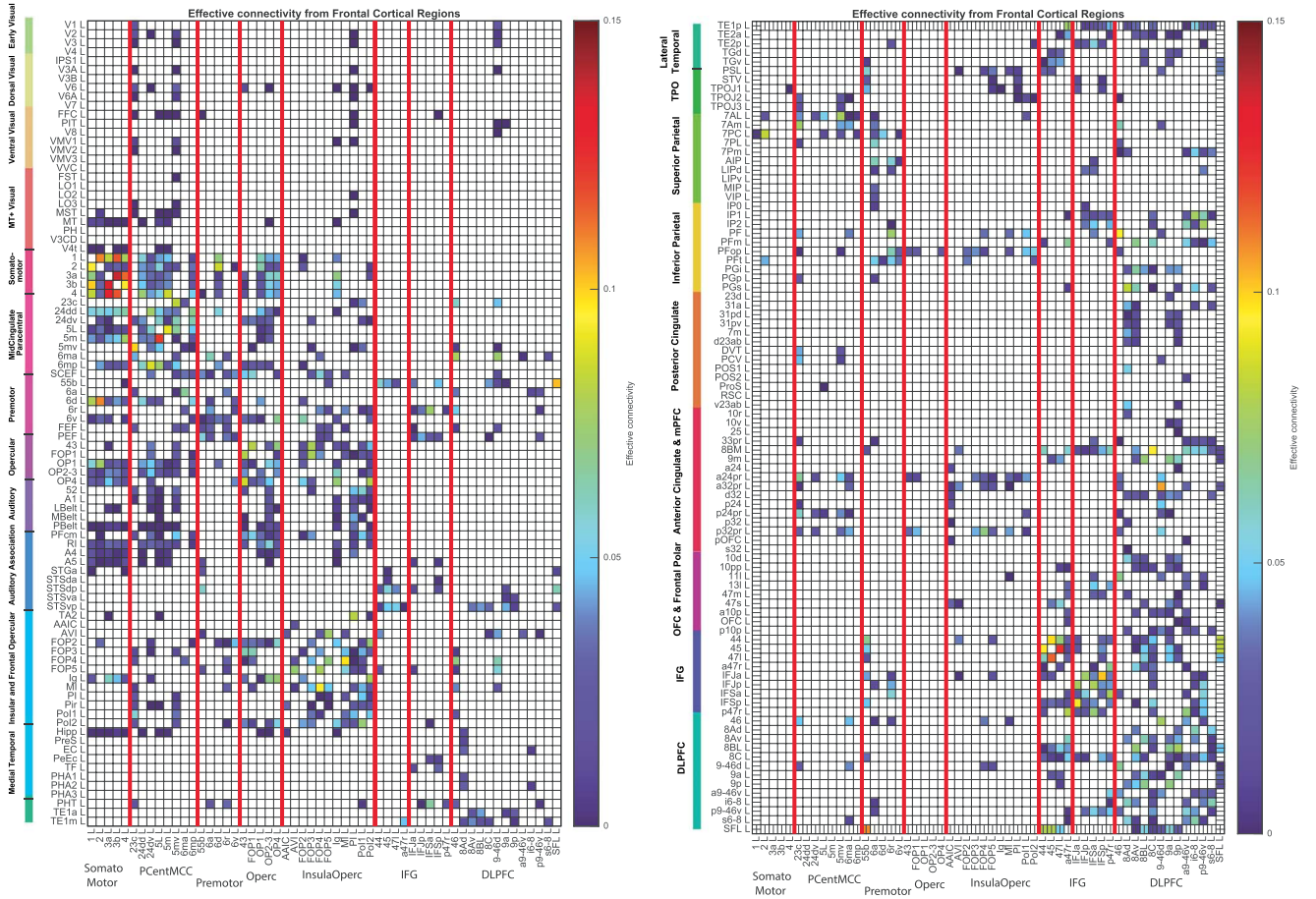

Fig. 3. Effective connectivity "FROM" the frontal cortical regions "TO" 180 cortical areas in the left hemisphere. The effective connectivity is read from column to row. effective connectivities of 0 are shown as blank. Abbreviations: see Table S1. The divisions of frontal cortex areas are separated by red lines.

visuo-motor parietal area 7, intraparietal, and inferior parietal regions (PF).

Paracentral and midcingulate cortex division (5L, 5m, 5mv, 6ma, and 6mp; 23c, 24dd, and 24dv in the midcingulate motor area)

The effective connectivity of the midcingulate cortex has been described previously (Rolls, Wirth, et al. 2022h) and is not dealt with in detail here. The area 5 regions are postcentral and considered as somatosensory, and the area 6 regions are precentral and considered premotor. The effective connectivity of one of these regions, 5mv, is shown schematically in Fig. 8.

Region **5L** receives effective connectivity moderately from 2 (0.034), less from 3b (0.013), less from 1 (0.008), and not from 3a (Figs. 2–4). This is consistent with the hypothesis that 5L is above 2 in a somatosensory hierarchy. Region 5L also receives from 7AL (0.076), and the supracallosal anterior cingulate p24pr, and has strong connectivity with 5m and 5mv. Region 5L has stronger effective connectivity to OP1-3 and the retroinsular area RI than from them and has effective connectivity to 4, 6mp and 6d, and MCC (24dd and 24dv).

Region **5m** receives effective connectivity from 3b, 3a, 1 and 2, 5L (0.12), and OP2-3. It has effective connectivity to 4 and 24dd (Figs. 2–4). There is weak effective connectivity from V2 (0.01).

Region **5mv** has effective connectivity with 5L, 7AL, 7Am, and the supracallosal anterior cingulate (a23pr, p24pr, and p32pr). Region 5mv has connectivity to 6mp, the midcingulate premotor cortex (23c, 24dd, and 24dv), and, less strongly, to the eye fields (FEF and SCEF), to the insula (RI and PoI1-2), and has connectivity directed to inferior parietal PFcm (0.05). There is some effective connectivity with visual areas (V1, V2, V6, and VMV1) and with auditory 52. Region 5mv also has some connectivity to multimodal-/language-related regions TPOJ2-3 (Rolls, Deco, et al. 2022d) and to posterior cingulate division regions DVT and PCV (Rolls, Wirth et al. 2022h) (Figs. 2–4).

Region **6ma** has effective connectivity from 5mv and FOP4; and also from 7Am, 7AL, and 7Pm; PF; the supracallosal anterior cingulate (a23pr, p24pr and p32pr); 23c in the MCC; the DLPFC (46, 9-46d); and the medial orbitofrontal cortex 11l. It also has effective connectivity with 6a and 6r.

Region **6mp** has effective connectivity from somatosensory regions 2, 3a, 3b, 5L, and 5mv and some from frontal opercular area 1 (FOP1) and OP1-3; and also from 7AL and 7Pc; PFcm; the supracallosal anterior cingulate (p24pr); and midcingulate 24dd and 24dv. It also has effective connectivity with 6d. It has connectivity to primary motor cortex 4.

Premotor division (55b, 6a, 6d, 6r, 6v)

Region **6a** receives strong effective connectivity from 7AL, 7Am, 7PC, and 7PL and receives moderate effective connectivity from some intraparietal regions (AIP, LIPd, MIP, and VIP). It also receives from PF, PFt, and PGp. Region 6a can thus be considered as

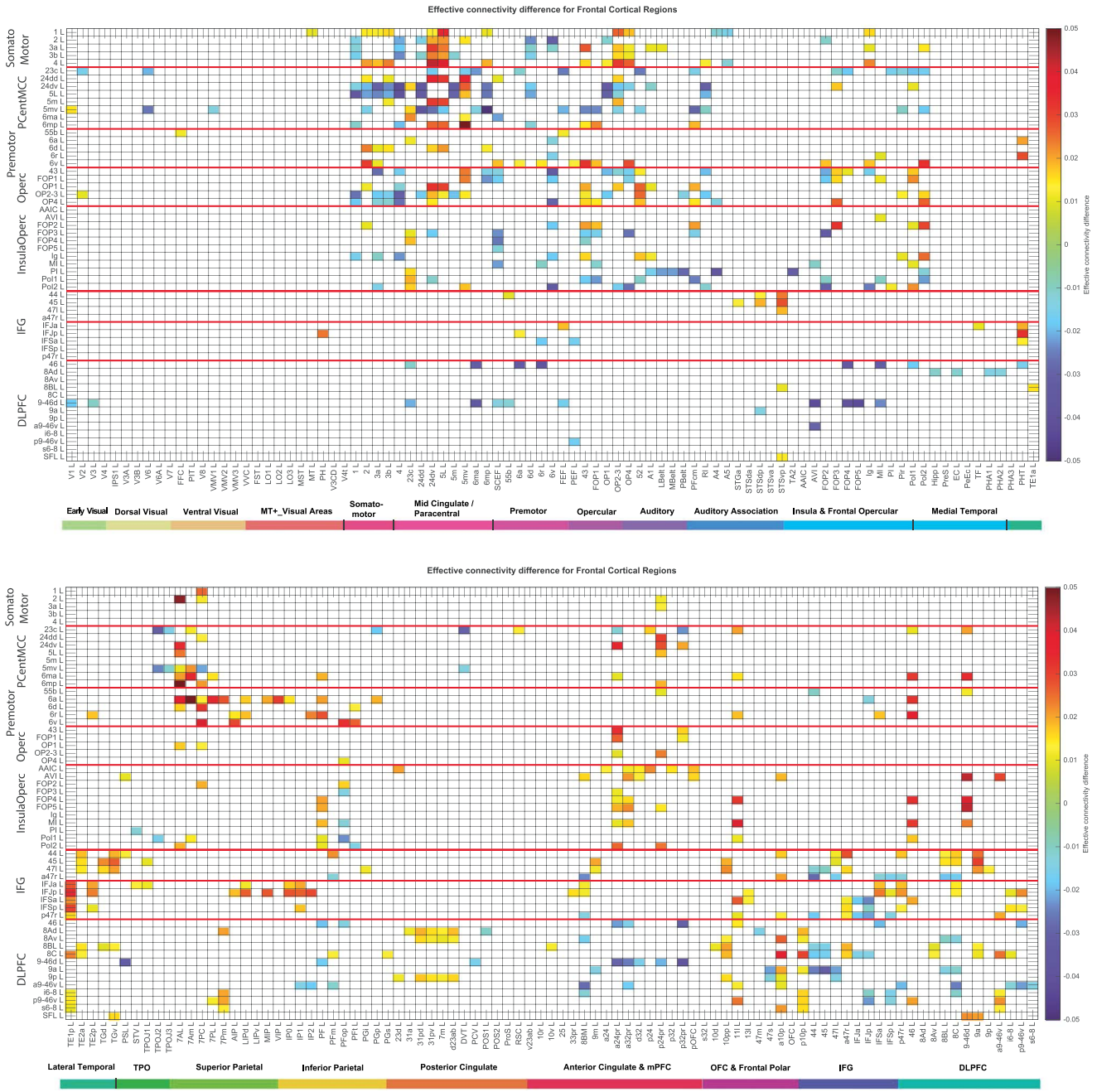

Fig. 4. Difference of the effective connectivity for frontal cortical regions with other cortical regions. For a given link, if the effective connectivity difference is positive, the connectivity is stronger in the direction from column to row. For a given link, if the effective connectivity difference is negative, the connectivity is weaker in the direction from column to row. This is calculated from 171 participants in the HCP imaged at 7T. The threshold value for any effective connectivity difference to be shown is 0.01. The abbreviations for the brain regions are shown in Table S1, and the brain regions are shown in Fig. 1 and Fig. S1. The effective connectivity difference for the first set of cortical regions is shown in the top panel; and for the second set of regions, it shown in the lower panel. Conventions as in Fig. 1.

an important premotor region for the visual motion and visuomotor outputs of the parietal cortex. It also has some effective connectivity from PHT in the posterior inferior temporal visual cortex and the DLPFC (46 and p9-46v). Region 6a has effective connectivity with 6ma and 6r (Figs. 2–4).

Region **6d** has effective connectivity from somatosensory 1, 2 (strong 0.10) and 3b, 3a and OP1 (moderate 0.04), and 5L. It also receives from 7PC and PFt. It has effective connectivity with 6mp and 6v and with MCC 24dd and with primary motor cortex 4.

Region **6r** has effective connectivity from FOP4 and the middle insula (MI); from AIP and LIPd; from PF (0.10), PFop and PFt; from inferior
temporal visual PHT and TE2p; and from the eye fields FEF, PEF, and SCEF. Region 6r also receives from medial orbitofrontal cortex 11l and from DLPFC 46. Region 6r also has moderate effective connectivity with 6a and 6v.

Region **6v** receives from somatosensory 2, 3a, 43, FOP1-2, OP4, and insula Ig and posterior insula region 2 (PoI2). Region 6v also

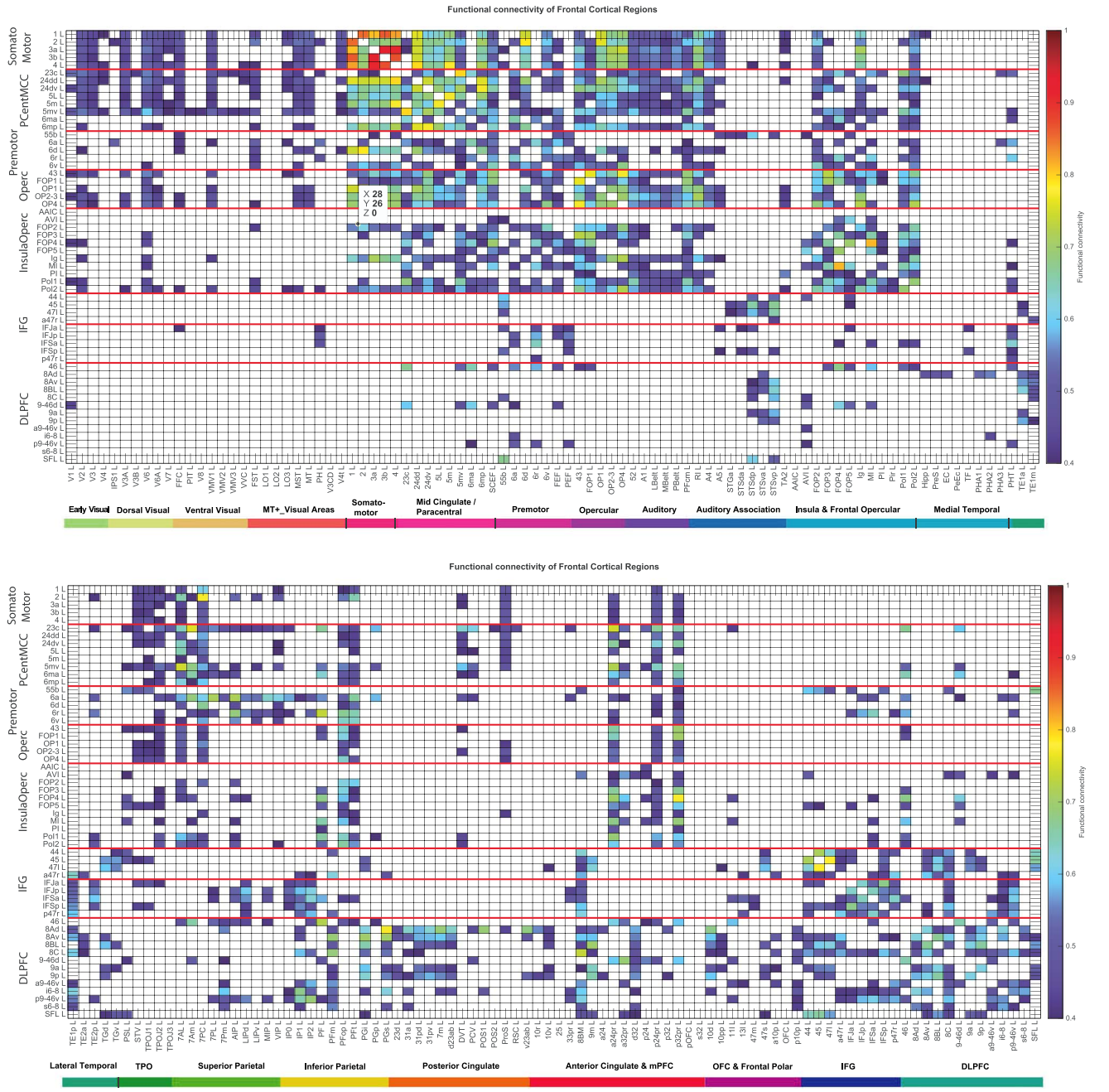

Fig. 5. FC between frontal cortical regions and 180 other cortical regions in the left hemisphere. FCs <0.4 are shown as blank. The upper figure shows the FC of the frontal cortical regions with the first half of the cortical regions; the lower figure shows the FC with the second half of the cortical regions. Abbreviations: see Table S1. Conventions as in Fig. 1.

receives from 7PC, AIP, PF, and PFt. It has effective connectivity with 6d and 6r.

Region **55b** is somewhat different, is sandwiched between the FEF and PEF (Fig. 1), and has strong connectivity with the language connectome (Rolls, Deco, et al. 2022d). It has effective connectivity from the FEF, PEF, and SCEF; with language-related regions STSdp, TGv, PSL, STV, TPOJ1, and superior frontal language region (SFL); and with Broca's area 44, 45, and the associated regions IFJa and IFSp and 47l (Figs. 2–4). It has weak effective connectivity with auditory A5. It may be a language-related output region for the control perhaps of eye movements or of the larynx (Rolls, Deco, et al. 2022d).

Posterior opercular division (43, FOP1, OP1-SII, OP2-3-VS, and OP4-PV)

These are probably mainly somatosensory cortical regions at the inferior end of the somatosensory cortex that continue into the opercular region, and, given their location, are likely to be involved in somatosensory processing of the face and nearby regions.

Region **43** has strong effective connectivity with FOP1, OP4, FOP3, and PoI2 and receives from 5mv, with some visual input from V6, auditory from 52, and input from supracallosal anterior cingulate a24pr and p32pr (Figs. 2–4). Region 43 has connectivity to primary motor cortex 4, to premotor 6mp and 6v, and to the granular insula (Ig). Region 43 also has connectivity with parietal

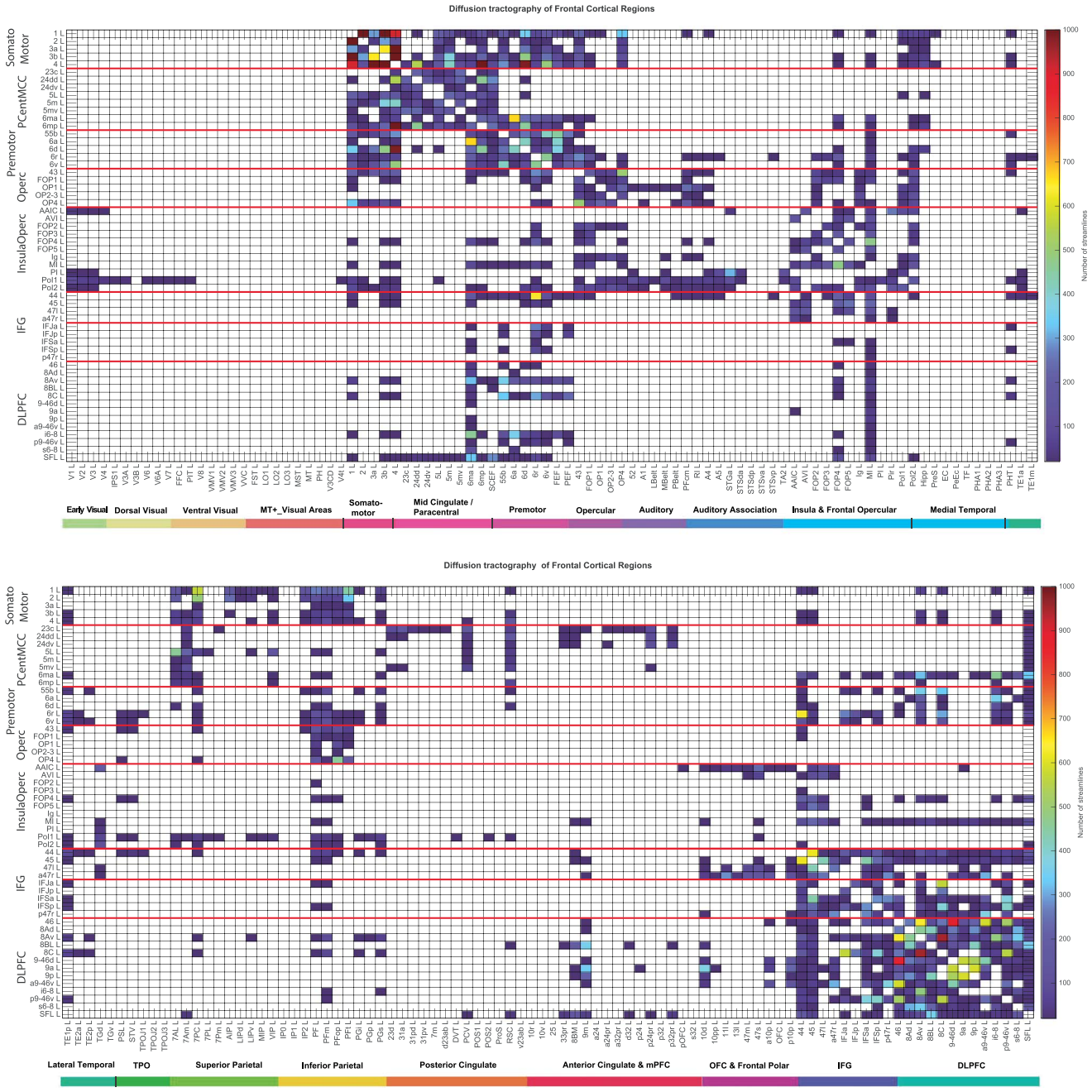

Fig. 6. Connections between the frontal cortical regions and 180 other cortical regions in the left hemisphere as shown by diffusion tractography using the same layout as in Figs. 1 and 4. The number of streamlines shown was thresholded at 10 and values less than this are shown as blank. The color bar was thresholded at 1,000 streamlines (see text). Abbreviations: see Table S1. Conventions as in Fig. 1.

PFcm and PFop, thereby providing inputs to the inferior parietal somatosensory hierarchy which culminates in PF (Rolls, Deco, et al. 2022b).

Region **FOP1** receives from 5mv, supracallosal anterior cingulate a24pr and p24pr, and insula MI, posterior insula region 1 (PoI1), and PoI2; has effective connectivity with 43 and FOP2-4; and has effective connectivity to premotor 6mp, 6v, and MCC 24dv.

Region **OP1** receives effective connectivity from 2 > 1 > 3b > 3a > 43, 5L, LOP2-3, OP4, and FOP2; and from parietal 7AL, 7PC and PFcm; and from auditory 52 and A1. OP1 has effective connectivity with OP2-4 and FOP2 and the retro-insula RI. OP1 has effective connectivity to 4, 6d, and 6mp and with MCC 24dd and 24dv.

Region **OP2-3** has effective connectivity that is stronger to 3a, 3b, 1, and 2 and 5m and OP1 and OP4. OP2-3 receives moderate effective connectivity from auditory 52, A1, Mbelt and Pbelt. OP2-3 has some effective connectivity from the supracallosal anterior cingulate cortex p24pr and a24pr. OP2-3 has moderate effective connectivity with insular regions RI, Ig, and PoI2. The is some effective connectivity to 6mp.

Region **OP4** has effective connectivity that is stronger to 3a, 3b, 1 and 2. OP2-3 has strong effective connectivity with 43, OP1, OP2-3, and FOP2-3. OP4 has effective connectivity from auditory 52 and to A4. OP4 has strong effective connectivity with insular IG and PoI2 and moderate with parietal PFcm and PFop. OP4 has effective connectivity to premotor 6v.

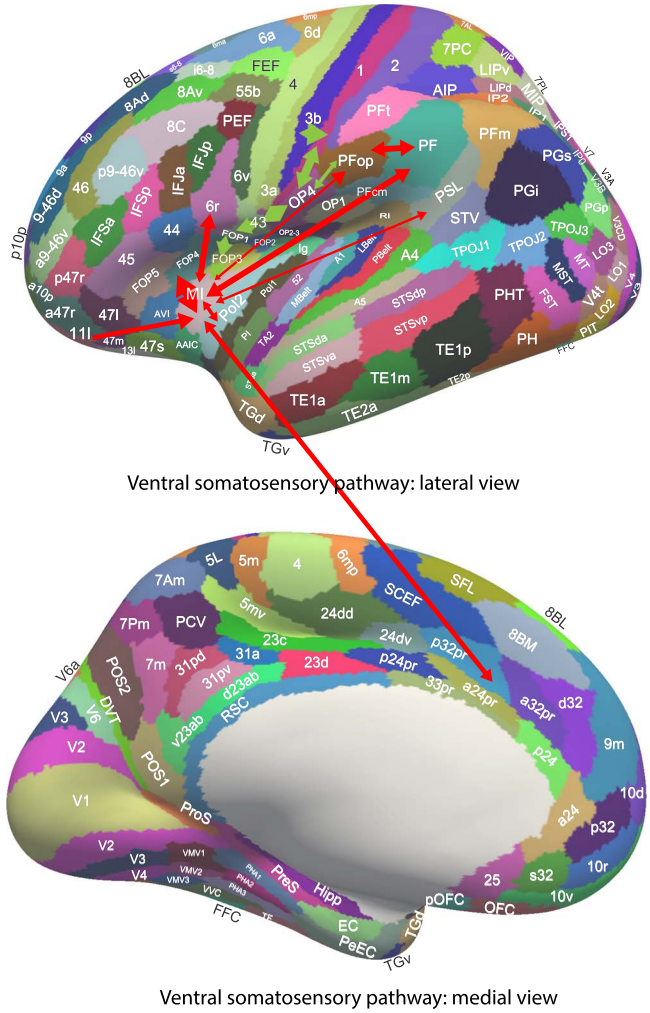

Fig. 7. Ventral somatosensory/insula stream effective connectivity. The connectivity from the primary somatosensory cortex 3b to the MI area is shown with green arrows. The onward connectivity of the MI to, for example, PF, the PSL, and the supracallosal anterior cingulate cortex p32pr, a32pr, and a24pr is shown with red arrows. The connectivity of the posterior insular region PoI2 is very similar to that of MI. The width of the arrows reflects the effective connectivity with the size of the arrowheads reflecting the connectivity in each direction. The pathway in more detail is as follows, where > reflects an effective connectivity but does not exclude effects across levels: (3b + 3a <> 1 + 2) <> OP4 <> 43 <> FOP1 <> FOP3 <> (MI + PoI2 + PoI1) <> PF + PFop. The abbreviations are listed in Table S1. The connectivity of PF and other posterior parietal cortex regions is described elsewhere (Rolls, Deco, et al. 2022b).

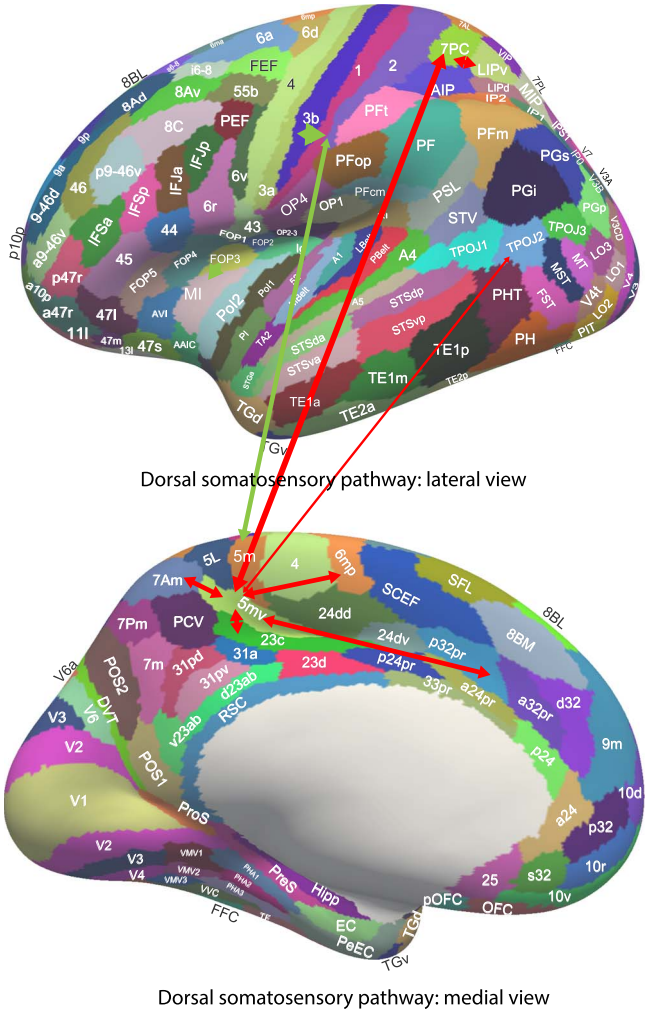

Fig. 8. Dorsal somatosensory stream effective connectivity. The connectivity from the primary somatosensory cortex 3b partly via 1 and 2 to area 5 somatosensory regions 5m > 5L > 5mv is shown with green arrows. The onward connectivity of the 5mv to, for example, posterior parietal 7AL, 7Am and 7PC which have connectivity with intraparietal regions, such as LIP, is shown with red arrows. The width of the arrows reflects the effective connectivity with the size of the arrowheads reflecting the connectivity in each direction. The pathway in more detail is as follows, where > reflects an effective connectivity but does not exclude effects across levels: (3b + 3a <> 1 + 2) <> 5m <> 5L <> 5mv <> 7AL, 7Am and 7PC. 5mv also has connectivity to 6mp, TPOJ2, and the supracallosal anterior cingulate cortex p32pr, a32pr, and a24pr.

Insula and frontal opercular division (anterior agranular insula complex AAIC; Anterior Ventral Insular area AVI; frontal opercular areas FOP2, FOP3, FOP4, and FOP5; the Ig; the Middle Insular area MI; para-insular area PI; posterior insular cortex PoI1, and PoI2)

The effective connectivity of one of these regions, the MI, is shown schematically in Fig. 7. The connectivity of PoI2 is very similar.

Anterior agranular insula complex (AAIC) in humans is a region in the ventral and anterior insula immediately posterior to lateral orbitofrontal cortex 47s (Fig. 1). It has effective connectivity with the pyriform olfactory cortex and with AVI which (with FOP3-5) is where the primary taste cortex is located (Rolls 2015, 2016a, 2016c). AAIC also receives from pOFC and pregenual anterior cingulate (a24, d32, and p32) and has effective connectivity with 47s.

AVI, part of the primary taste cortex, has connectivity with FOP4, FOP5, and AAIC and also with MI, 47s, and pOFC. It has strong connectivity with supracallosal anterior cingulate a32pr and some effective connectivity with pregenual anterior cingulate. Interestingly, it has effective connectivity with a number of language-related regions, including strongly with Broca's area 44, and some with the PeriSylvian Language area (PSL). AVI receives effective connectivity from frontal regions 8BM, 9-46d, and a9-46v.

FOP2 which is a little more posterior in the dorsal (superior) insula than the other FOP areas (Fig. 1) receives effective connectivity from FOP1 and FOP3 and 43; has effective connectivity with somatosensory 2, OP1 and OP4; and has effective connectivity to premotor 6v and 6d. FOP2 also receives from

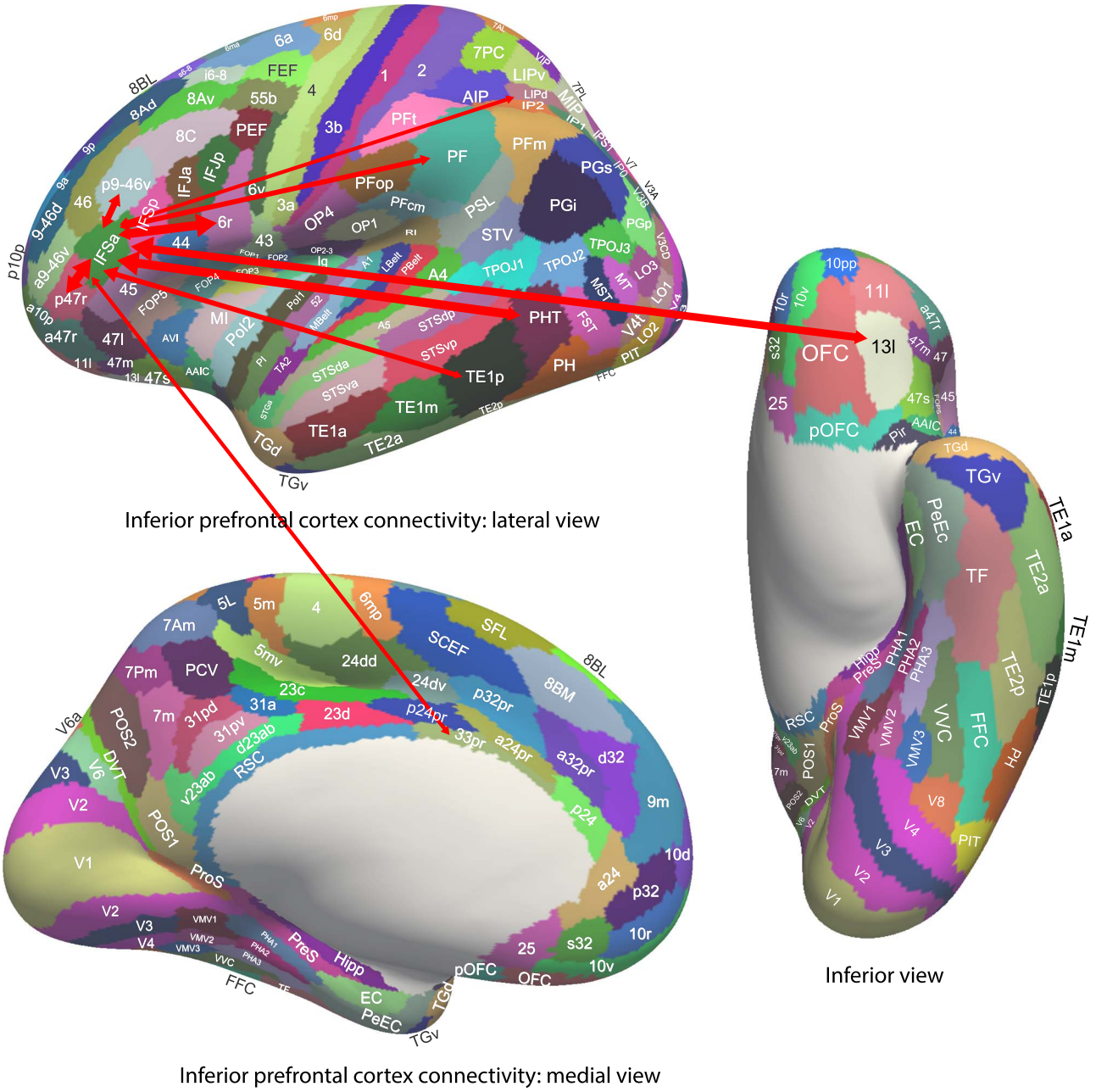

Fig. 9. Inferior prefrontal cortex effective connectivity. The connectivity of IFSa is shown as an example of the connectivity of IFja, IFJp, IFSa, and IFSp, with details shown in Figs. 2–4. The width of the arrows reflects the effective connectivity, with the size of the arrowheads reflecting the connectivity in each direction. The effective connectivity with the inferior temporal visual cortex (TE1p, TE2p, and PHT); and with the medial orbitofrontal cortex 13l and 11l; and the lateral orbitofrontal cortex p47r and a47r are notable. IFSa has moderate effective connectivity with the other IF regions.

insula Ig, PoI2, and PoI1 and from 7PC and 7AL. FOP2 also has moderate effective connectivity with PFop, PFt, and PFcm, which tends to be a little stronger from these parietal areas than to them. FOP2 has effective connectivity to premotor 6v and 6d.

FOP3 has effective connectivity with 43, FOP1, FOP2 and FOP4, and OP1 and OP4; with insular MI, PoI1, and PoI2; and with parietal PFcm and PFop. It receives weakly from PF, the top of the parietal somatosensory hierarchy. FOP3 also has effective connectivity with supracallosal anterior cingulate cortex a24pr and p32pr. It has some effective connectivity with the midcingulate motor area 24dv and 23c and has some effective connectivity to SCEF, the supplementary and cingulate eye field.

FOP4 has effective connectivity with FOP1, FOP3, FOP5, and AVI; with the MI; and with the supracallosal anterior cingulate cortex (p32pr, a24pr, and a32pr). FOP4 has quite strong effective connectivity with PF, and some with the PSL, and receives from the medial orbitofrontal cortex 11l. FOP4 receives more strongly from DLPFC 46 and 9-46d than it sends to them. FOP4 has connectivity to 6r and 6ma and to the eye fields SCEF, FEF, and PEF.

FOP5 has effective connectivity with FOP1, Fop3, FOP5, AVI, and the MI. FOP5 is connected with some language regions, including PSL, 44, and IFJa. It has effective connectivity with premotor regions 6r, 55b, SCEF, FEF, and PEF. FOP5 also has effective connectivity with supracallosal anterior cingulate cortex (a24pr, p24pr, a32or, and p32pr). FOP5 also receives from DLPFC 9-46d.

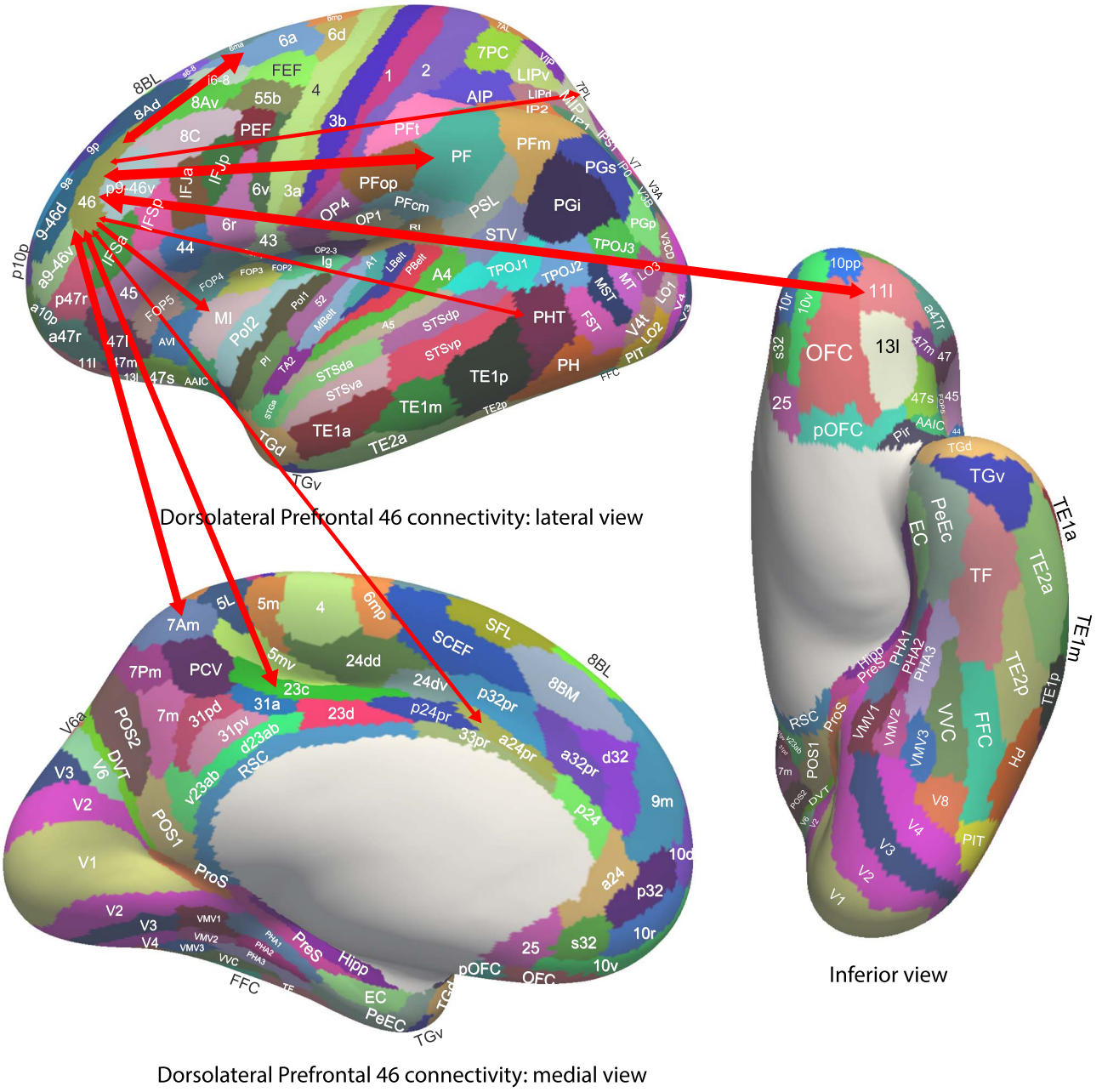

Fig. 10. Dorsolateral prefrontal cortex effective connectivity. The connectivity of region 46 is shown as an example of the connectivity of regions 46, 9-46d, a9-46v, and p9-46v, with details shown in Figs. 2–4. The width of the arrows reflects the effective connectivity with the size of the arrowheads reflecting the connectivity in each direction. The effective connectivity with the superior parietal cortex 7Am and 7PL, the strong connectivity with inferior parietal PF, and with the medial orbitofrontal cortex 11l are notable. 46 has moderate effective connectivity with the other DLPFC regions 9-46d, a9-46v, and p9-46v.

Ig, the granular insular region, is relatively posterior in the insula (Fig. 1). Ig has effective connectivity with somatosensory 3b, 3a, 1, 43, OP2-3, OP4, and FOP2 and to motor 4 and premotor 6v. Ig also has effective connectivity from some nearby auditory regions 52, A1 and from the pyriform (olfactory) cortex.

MI has effective connectivity with FOP3, FOP4, FOP5, and FOP1; with insular regions PI, PoI1, and PoI2; from PF and with PGop; with the supracallosal anterior cingulate cortex (a24pr, p32pr, and a32pr). MI receives moderate (0.04) effective connectivity from the medial orbitofrontal cortex 11l and from DLPFC 46 and 9-46d. It has effective connectivity to 6r, SCEF, and FEF. It has weak effective connectivity to AVI.

PI, the para-insular region, an antero-ventral region of the insula, has PoI2 just dorsal to it, and auditory 52 just posterior (Fig. 1). PI has effective connectivity with POI1 and to the mid-cingulate premotor region 23c, supracallosal anterior cingulate a24pr, and FOP5. However, it has moderate effective connectivity with auditory cortex regions, including, especially 52, MBelt, and PBelt, and has strong effective connectivity to auditory TA2 and moderate to A4. It has weak effective connectivity to language regions PSL and STV.

PoI1 has moderate effective connectivity with somatosensory FOP3, 5mv, MI, PI, and PoI2, and some effective connectivity with FOP1 and 43, and supracallosal anterior cingulate a24pr and p24pr. It has strong effective connectivity with PF and PFop. PoI1

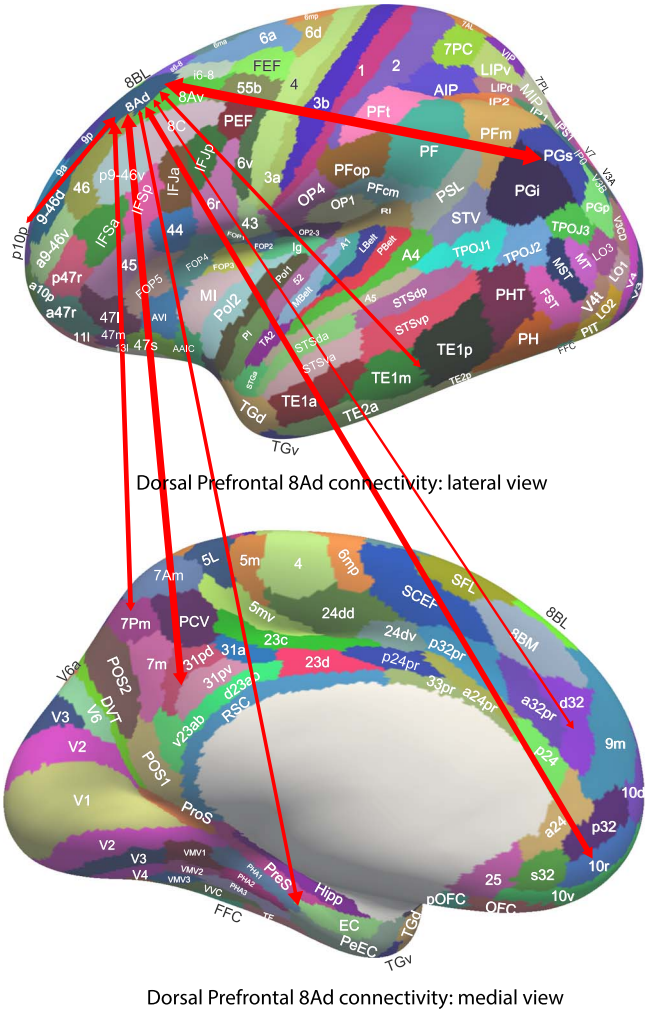

Fig. 11. Dorsal prefrontal cortex effective connectivity. The effective connectivity of region 8Ad is shown as an example of the connectivity of regions 8Ad, 8Av, 9p, i6-8, and s6-8, with details shown in Figs. 2–4. The width of the arrows reflects the effective connectivity, with the size of the arrowheads reflecting the connectivity in each direction. The effective connectivity with the inferior parietal PGs and PGi and with 7Pm are notable. There is also connectivity with the entorhinal cortex (EC) and parahippocampal gyrus regions PHA1-2, and with the memory-related parts of the posterior cingulate division (31pd, 31pv, v23ab), and 7m. 8Ad also has some connectivity with TE1m and TE1p. 8Ad also has some connectivity with reward-related regions, the ventromedial prefrontal cortex 10d and 10r, and the pregenual anterior cingulate cortex d32, p32 (Rolls, Deco, et al. 2022f). 8Ad has moderate effective connectivity with the other dorsal prefrontal regions 8Av, 9p, i6-8 and s6-8.

receives effective connectivity from 7AL and 7Am. PoI1 also has strong effective connectivity with auditory region 52. POI1 also receives from the medial orbitofrontal cortex (11l) and from the DLPFC region 46.

PoI2 has moderate effective connectivity with somatosensory 43, OP2-3, OP4, FOP2, and FOP3. PoI2 receives from supracallosal anterior cingulate (a24pr and p24pr) and from 7AL. PoI2 has effective connectivity with other insular regions (Ig, MI, PI, and RI) and with PF. PoI2 has some effective connectivity with auditory 52 and has effective connectivity toward premotor 6v and 6r. PoI2 also has effective connectivity to inferior parietal PFop and PFt, and this contributes to connecting the somatosensory and opercular somatosensory regions to the parietal somatosensory hierarchy (Rolls, Deco, et al. 2022b).

Inferior frontal gyrus (regions 44, 45, 47l, a47r, IFJa, IFJp, IFSa, IFSp, and p47r)

The effective connectivity of one of these regions, the inferior frontal sulcus anterior IFSa region, is shown schematically in Fig. 9.

Regions 44 and 45 on the left are Broca's area, have strong effective connectivity with 47l, and have been considered in detail when considering the human language connectome (Rolls, Deco, et al. 2022d) and so are considered only briefly here. (A red line separates them and a47r from the other members of this division in the figures in this paper.)

Region **44** receives effective connectivity from STSdp and STSvp, which are parts of the superior and inferior superior temporal sulcus (STS) semantic systems (Rolls, Deco, et al. 2022d). Region 44 also receives effective connectivity from other language-related regions, including TGv and PSL. Region 44 also has moderate effective connectivity with the nearby IFJa and IFSp and has strong effective connectivity with 45 and with 47l. Region 44 receives from a47r and p47r, which are nominally parts of the lateral orbitofrontal cortex. Region 44 has moderate effective connectivity with somatosensory FOP5 and with taste AVI. It also receives from TFm. Region 44 also receives from inferior temporal visual cortex TE2a and from DLPFC regions 8BL, 8C, and 9a. Region 44 also has strong effective connectivity with premotor 55b and with the Superior Frontal Language region SFL.

Region **45** receives effective connectivity from STSdp and STSvp and from further language areas STGa, STSda, TGv, TGd, PSL, 47l, 47s, and TPOJ1. Region 45 also receives from frontal pole 10pp, lateral orbitofrontal a47r, and from dorsal prefrontal regions 8BL, 8C, 9a, and 9p. Region 45 also has strong effective connectivity with 44, premotor 55b, and with the SFL.

Region **47l** is very strongly connected with 45 (0.12) and with 44 (0.07). It appears as if, in humans, this part of what is nominally part of the lateral orbitofrontal cortex, is being used for language-related functions (Rolls, Deco, et al. 2022d). Consistent with this, 47l receives from STSdp, STSvp, TGv, TGd, and PGi. Region 47l also receives from TE2a, frontal pole 10pp, and dorsal prefrontal 8BL, 8C, 9a, and 9p. Region 47l has effective connectivity with inferior frontal gyrus region IFSp. Region 47l receives from a47r. Region 47l has effective connectivity to premotor 55b, and with the SFL.

a47r is part of the human lateral orbitofrontal cortex. a47r has effective connectivity with the inferior temporal visual cortex TE1m, TE1p, and TE2a; with the visual inferior parietal cortex PFm; with the medial orbitofrontal cortex regions OFC and 13l; and with lateral orbitofrontal cortex 47l and p46r. a47r has effective connectivity to 44 and 45 and to IFSa and IFSp and to the dorsal prefrontal cortex 8Av, 8Ad, and 8C.

Next, there is a series of inferior frontal gyrus regions with interesting connectivity with Broca's 44 and 45. It has been proposed that these IF regions provide an extension to Broca's region to provide for more attractor-based networks that may be involved in syntax (Rolls, Deco, et al. 2022d).

IFJa receives effective connectivity from inferior temporal visual cortical regions, including TE2p, TE1p, PHT, and parahippocampal TF; from some intraparietal visual motion-related regions (LIPd, IP0, and IP1); and from lateral orbitofrontal cortex region p47r. IFJa has strong effective connectivities with IFJp and IFSp and some effective connectivity with 44 and 45 and other language regions TPOJ1, STV, and 55b. IFJa also receives from dorsal prefrontal 8C and i6-8. IFJa has effective connectivity with premotor 55b, 6r, and with the frontal eye field FEF. IFJa is thus implicated in language-related processing with visual inputs.

IFJp receives effective connectivity from inferior temporal visual cortical regions, including TE2p, TE1p, and PHT; from some intraparietal grasp/motion-related regions (AIP, LIPd, MIP, IP0, IP1, and IP2); from lateral orbitofrontal cortex region p47r; and from medial orbitofrontal 13l. IFJp has strong effective connectivities with IFJa, IFSa, and IFSp. IFJp also receives from dorsal prefrontal 8C and i6-8 and p9-46v. IFJa has effective connectivity with premotor 6a and 6r and with the premotor eye field PEF. IFJp does not have connectivity with language-related regions, and thus appears to be a region related to visual short-term memory, especially for objects.

IFsa receives effective connectivity from inferior temporal visual cortical regions, including TE2p, and TE1p, and from parahippocampal TF; from intraparietal grasp/motion-related regions (AIP, LIPd, IP1, and IP2); from lateral orbitofrontal cortex regions p47r and a47r; and from medial orbitofrontal 13l and 11l. IFsa has strong effective connectivities with IFJa, and IFJp. IFsa also receives from DLPFC 46v and p9-46v. IFsa has effective connectivity to premotor 6r and the premotor eye field PEF. IFsa also does not have connectivity with language-related regions, and thus appears to be a region related to visual short-term memory, especially for objects, and to reward/punishment value from the orbitofrontal cortex.

IFsp receives effective connectivity from inferior temporal visual cortical regions, including TE2p, TE1p, and PHT; from intraparietal IP1; and from lateral orbitofrontal cortex regions p47r and a47r. IFsp has strong effective connectivities with IFJa and IFJp and IFsa. IFsp also receives from dorsal prefrontal 8C, i6-8, and p9-46v. IFsa has effective connectivity to premotor 55b and the premotor eye field PEF. IFsa also does not have connectivity with language-related regions, and thus appears to be a region related to visual short-term memory, especially for objects.

p47r receives effective connectivity from inferior temporal visual cortical regions, including TE1p, TE2a, and PHT; from intraparietal IP1 and IP2; from PFm which is visual (Rolls, Deco, et al. 2022b); from lateral orbitofrontal cortex region a47r; and from medial orbitofrontal 11l and 13l. p47r has strong effective connectivities with IFsa and moderate with IFJa and IFJp and IFsp. p47r also has effective connectivity with DLPFC a9-46v, p9-46v and 8C. p47r has effective connectivity to 8BM and 44. p47r is activated by punishers and nonreward and may be involved in pairing visual inputs with reward/punishment value and thereby in emotion (Rolls 2019a, 2019b; Rolls, Deco, et al. 2022f).

Dorsolateral prefrontal cortex division (46, 8Ad, 8Av, 8BL, 8C, 9-46d, 9a, 9p, a9-46v, i6-8, p9-46v, and s6-8)

As noted in the Introduction, the DLPFC regions are implicated in short-term memory (Funahashi et al. 1989; Goldman-Rakic 1996; Goldman-Rakic and Leung 2002) and thereby in executive function for internally generated actions (Fuster 2021; Passingham 2021; Rolls 2021c) and top-down attention (Deco and Rolls 2004; Deco and Rolls 2005a; Deco and Rolls 2005b). In the following, some distinction is made between regions, such as 46 in the DLPFC, and regions 8..., which are dorsal prefrontal regions.

The effective connectivity of one of these regions, 46 as an example of a dorsolateral prefrontal region, is shown schematically in Fig. 10; and of another region, 8Ad as an example of a dorsal prefrontal region, in Fig. 11.

Region **46** receives from parietal 7Am, 7PL, and PF. It has effective connectivity also from the medial orbitofrontal cortex 11l. Region 46 has effective connectivity with other DLPFC regions 9-46v, a9-46v, and p9-46v. Region 46 has effective connectivity to premotor regions 6ma, 6a, 6r, and midcingulate 23c. Region 46 also has effective connectivity to somatosensory FOP4 and insular MI and PoI1, to supracallosal anterior cingulate a24pr and a32pr which are also somatosensory/action (Rolls, Deco, et al. 2022f), to visual PHT, and to IFsa, which may be for top-down control.

Region **8Ad** has moderate effective connectivity from parietal PGs, PGi, and 7Pm; weaker from visual inferior temporal TE1p and TE1m; from reward-related vmPFC 10r and 10v and pregenual anterior cingulate d32 and p32; and from frontal pole p10p. Region 8Ad has effective connectivity with other dorsal prefrontal regions 8Av, 9p, i6-8, and s6-8. Region 8Ad has interesting effective connectivity with the episodic memory system; to parahippocampal PHA1 and PHA2, entorhinal cortex (EC), presubiculum, and hippocampus (Rolls 2022a; Rolls, Deco, et al. 2022e); and with memory-related posterior cingulate cortex regions 31pd, 31pv, 7m, and v23ab; and also with posterior cingulate 31a, d23ab and POS1 (Rolls, Wirth, et al. 2022h).

Region **8Av** has moderate effective connectivity from parietal PFm, PGs, and PGi; some too from visual inferior temporal TE1a, TE1m, TE1p, and TE2a; from reward-related vmPFC 10d and pregenual anterior cingulate d32 and 9m; with lateral orbitofrontal a47r; and from frontal pole 10pp, a10p, and p10p. Region 8Av has effective connectivity with other dorsal prefrontal regions 8Ad, 8BL, 8C, 9a, and 9p. Region 8Av has effective connectivity with memory-related posterior cingulate cortex regions 31pd, 31pv, 7m; and also with posterior cingulate d23ab (Rolls, Wirth, et al. 2022h). Region 8Av thus differs from 8Ad in that 8Ad has more connectivity with the hippocampal memory system; and 8Av has more visual parietal and visual inferior temporal cortex connectivity.

Region **8BL** has moderate effective connectivity from inferior temporal visual cortex TE1a, TE1m, and TE2a; from temporal pole TGd and TGv; from parietal PGi; from reward-related vmPFC 10v and 10d and pregenual anterior cingulate d32 and 9m; with lateral orbitofrontal a47r and 47l; and from frontal pole 10pp. Region 8BL also has effective connectivity with STSvp, which is part of the ventral STS semantic system (Rolls, Deco, et al. 2022d). Region 8BL has effective connectivity with other dorsal prefrontal regions 8Av, CL, 9a, and 9p.

Region **8C** has moderate effective connectivity from inferior temporal visual cortex TE1p, TE1m, and TE2a; from visual inferior parietal PFm, PGi, and PGs; from IP1 and IP2; from lateral orbitofrontal a47r and p47r; and from frontal pole 10pp, a10p and p10p. Region 8C also has effective connectivity with STSvp, which is part of the ventral STS semantic system (Rolls, Deco, et al. 2022d). Region 8C has outputs to premotor language-related 55b, 44, 45, and SFL. Region 8C has effective connectivity with other dorsal prefrontal regions 8Av, 8BL, 9a, a9-46v, i6-8, and p9-66v.

Region **9-46d** has strong effective connectivity with supracallosal anterior cingulate a32pr and a24pr; from medial orbitofrontal cortex 11l; with the frontal pole a10p and p10p; with pregenual anterior cingulate d32; with 7Am; and to somatosensory FOP4, FOP5, MI, and taste AVI. Region 9-46d has effective connectivity to premotor 6ma and MCC 23c and to SCEF, FEF and 55b. Region 9-46d has effective connectivity with other DLPFC regions 46 and a9-46v.

Region **9a** has some effective connectivity from language-related temporal pole TGd and TGv, with STSvp, and to 45, 44, 47l, and 47s. Region 9a also has effective connectivity with visual inferior parietal PGi; from lateral orbitofrontal a47r and p47r; and from frontal pole 10pp, a10p and p10p. Region 9a has effective connectivity with other dorsal prefrontal regions 8Av, 8BL, 98C, and 9p. Region 9a also has some effective connectivity with the

memory-related parts of the posterior cingulate cortex 31pv and 31pd and with the pregenual anterior cingulate cortex d32 and 9m.

Region **9p** has effective connectivity with inferior parietal PGi and PGs (which are visual regions; Rolls, Deco, et al. 2022b); with visual inferior temporal cortex TE1a and TE1m; with temporal pole TGd and STSva and STSvp, which are part of a semantic system for visual stimuli, and to lateral orbitofrontal cortex 47s, 47l, and 45, and the SFL (Rolls, Deco, et al. 2022d); and with memory-related parts of the posterior cingulate and medial parietal cortex (31pd, 31pv, v23ab, and 7m (Rolls, Wirth, et al. 2022h); and from the frontal pole 10pp, a10p, and p10p. Region 9p also has effective connectivity with vmPFC 10d and 10v, pregenual anterior cingulate d32, and 9m. Region 9p has effective connectivity with other lateral prefrontal regions 8Ad, 8Av, 8BL, and 9a.

Region **a9-46v** has effective connectivity with inferior parietal visual PFm, IP2 and IP1, and superior parietal 7Pm. a9-46v also has moderate effective connectivity with medial orbitofrontal cortex 11l and 13l and lateral orbitofrontal cortex p47r. a9-46v has effective connectivity with the frontal pole a10p and p10p. a9-46v has effective connectivity to the insular AVI region. a9-46v has effective connectivity with other prefrontal regions 46, 8C, 8BM, 9-46d, i6-8, p9-46v, and s6-8.

i6-8 has effective connectivity with inferior parietal visual PFs, PFm, IP1, and IP2; with intraparietal LIPd and superior parietal 7Pm; and with TE1p. i6-8 has effective connectivity with the frontal pole p10p. i6-8 has effective connectivity to some inferior frontal gyrus regions IFJa, IFJp, and IFSp. i6-8 has effective connectivity with other prefrontal regions 8Ad, 8Av, 8C, a9-46v, and p9-46v.

p9-46v has effective connectivity with inferior parietal visual IP2, IP1, and PFm and to superior parietal 7Pm and 7PL. p9-46v also has moderate effective connectivity from medial orbitofrontal cortex 11l and 13l and with lateral orbitofrontal cortex p47r. p9-46v has effective connectivity from the frontal pole p10p. p9-46v has effective connectivity with some inferior frontal gyrus regions IFJp, IFsa, and IFSp. p9-46v has effective connectivity with other DLPFC regions 46, 8C, a9-46v, and i6-8.

s6-8 has effective connectivity with inferior parietal visual PFm, PGs, and superior parietal 7Pm; and with TE1p and TE1m. s6-8 has effective connectivity from the frontal pole p10p and a10p. s6-8 has effective connectivity with pregenual anterior cingulate d32. s6-8 has effective connectivity with other prefrontal regions 8Ad, 8Av, 8C, a9-46v, and p9-46v and i6-8.

Effective connectivities of the 57 frontal and related regions with contralateral cortical regions

The effective connectivities of the 57 regions from contralateral cortical areas are shown in Fig. S2 and to contralateral cortical regions in Fig. S3.

Differences of effective connectivities of the right versus left hemisphere for the 57 frontal and related regions

Most of the analyses presented so far have been for the left hemisphere, or of the left hemisphere with the right hemisphere. For completeness, the differences of effective connectivity for the right "minus" the left hemisphere for the 57 frontal and related cortical regions are shown in Figs. S6 and S7.

Correlations between the connectivities of different cortical regions

Figure S4 shows the correlations between the effective connectivities of the regions described here, and Fig. S5 shows the correlations between FCs. These correlation maps help to show which regions have similar effective connectivity, and which are different.

Discussion

The aim of the Discussion is to draw out the implications for the organization and operation of frontal cortical regions from the effective connectivities complemented by the FC and diffusion tractography described here. The strengths of the effective connectivities are used as a guide and so is evidence from neuronal recordings in comparable regions in macaques and neuroimaging activation studies in humans. The point made earlier that effective connectivity in the backward direction in a cortical hierarchical system does not reflect the transfer of the properties represented at a higher level, but instead the capability for top-down attention and for memory recall is borne in mind.

Somatosensory/motor frontal cortical regions including the insula

Physiological investigations in primates show that areas 3b and 1 represent cutaneous somatosensory information, with area 1 having larger receptive fields, that area 3a represents proprioceptive information, and that neurons in area 2 can respond to cutaneous or proprioceptive information or both in primates (Delhaye et al. 2018). As in humans, the legs are represented at the superior end of the somatosensory cortices 3a-2 and the face at the inferior end close to the operculum (Delhaye et al. 2018). In macaques, ventral to 3a-2 in the operculum are areas S2 and "parietal ventral" which are described as a ventral somatosensory stream (Mishkin 1979; Delhaye et al. 2018). In macaques, the pathways to 5 and 7b are described as a dorsal somatosensory stream to the posterior parietal cortex (Mishkin 1979; Gardner 2008; Delhaye et al. 2018). Several somatosensory processing streams may be present in humans (de Haan and Dijkerman 2020).

A ventral somatosensory stream

First, it is proposed that in humans there is a ventral somatosensory stream that connects via frontal opercular (FOP) regions to the insula which in turn has connectivity to the inferior parietal cortex PF regions, as illustrated in Fig. 7, as based on the effective connectivities shown in Figs. 2–4. The connectivity from the primary somatosensory cortex 3b to the MI is shown with green arrows in Fig. 7. The onward connectivity of the MI to, for example, PF, the PSL, and the supracallosal anterior cingulate cortex, p32pr, a32pr, and a24pr, is shown with red arrows. The connectivity of the posterior insular region PoI2 is very similar to that of MI. The pathway in more detail is as follows, where > reflects an effective connectivity but does not exclude effects across levels:

$$(3b + 3a <> 1 + 2) <> OP4 <> 43 <> FOP1 <> FOP3 <> (MI + PoI2 + PoI1) <> PF + PFop.$$

One of the interesting features of the connectivity shown in Fig. 7 is that it draws out the point that some of the opercular and the FOP regions can be considered as a continuation ventrally of somatosensory cortex regions 3a, 3b, 1, and 2 and with then a further ventral extension of the cortical sheet into the insula.

Another important feature is that this ventral stream is probably a "what" stream, for it does not have major connectivity with visuo-spatial action regions in area 7, but it does have connectivity with PFop and PF in which representations appear to be about the properties of objects and one's own body (Rolls, Deco, et al. 2022b). Indeed part of the function of these PF areas may be related to somatosensory/body image and the sense of body ownership and of self that this provides, which is consistent with evidence that anosognosia and other disorders of awareness of the body can be produced by PF damage in humans (Ronchi et al. 2018). Another interesting feature is that PF may on its connectivity evidence (Rolls, Deco, et al. 2022b) not only be the top of a somatosensory hierarchy but also adds visual and reward inputs to form semantic representations of felt objects, enabling recognition of, for example, a tool not only by its touch but also by its sight. Also consistent with the insula to PFop and PF stream being a "what" stream is that it also has access to language systems, via the PSL (Rolls, Deco, et al. 2022d), thus enabling verbal declarations to be made about what is felt, with declarative systems being "what" systems in the brain, whereas action systems are typically procedural and not declarative (Goodale and Milner 1992; Squire 1992; Milner and Goodale 1995; Squire and Zola 1996). Another feature of the connectivity is the very directional input from the reward-related (Grabenhorst and Rolls 2011; Rolls 2019a, 2019b) medial orbitofrontal cortex region 11l to the MI (Fig. 7), leading to the hypothesis that the somatosensory insula may encode some aspects of the reward or aversive value of somatosensory stimuli. Consistent with this, activation of the somatosensory insula was found by painful touch to the hand (Rolls et al. 2003), with a dorsal posterior insular region implicated in pain (Segerdahl et al. 2015).

An interesting property of insular function is that it was activated by touch to the arm, but not to the sight of touch to the arm, whereas the somatosensory cortical areas 1–3 responded to the sight of touch to the arm as well as to touch to the arm (McCabe et al. 2008). It was therefore suggested that the insula provides evidence that it is one's own body that is being touched, which might give it special status in body representations (McCabe et al. 2008; Craig 2009, 2011). Consistent with this, most of the insula (MI, PoI1, POI2, and also the FOP regions) does not receive connectivity from early cortical visual regions, whereas 3b, 3a, 1, 2, 5L, 5m, and 5mv do (Fig. 2). Another difference is that the somatomotor and paracentral areas have connectivity with parietal area 7 regions, whereas the insula does not; and the insula has more connectivity with inferior parietal PF regions than do the somatomotor and paracentral regions. Another difference is that as mentioned above the insula has connectivity directed toward language-related areas the PSL, STV, TPOJ1, and TPOJ2 (Fig. 3; Rolls, Deco, et al. 2022d), whereas the somatomotor and paracentral regions do not. These findings support the hypothesis that the insula is part of a ventral (or inferior) "what" stream of somatosensory processing that continues into inferior parietal cortex PF regions (Fig. 7); whereas as described next a dorsal (or superior) "action" stream of processing connects from somatomotor (areas 3b, 3a, 1, and 2) and paracentral (area 5) cortical regions to posterior parietal cortex area 7 and thereby intraparietal regions (Fig. 8).

The supracallosal part of the anterior cingulate cortex is implicated in action-outcome learning, with information about the actions that have been performed available from the somatosensory/motor regions described here and about the reward outcome received after an action being provided via the pregenual anterior cingulate cortex (Rolls, Deco, et al. 2022f). The connectivity described here implicates the insula in this circuitry, and the effective connectivity from the reward-related medial orbitofrontal cortex 11l (Fig. 2) to the insula could provide reward outcome information to enable the insular cortex to also be involved in action-outcome learning. Consistent with this hypothesis, the insular cortex does have some connectivity to premotor cortex 6 regions and to the midcingulate motor region (Fig. 3).

A dorsal somatosensory stream

A diagram of a dorsal somatosensory stream connecting via somatosensory area 5 regions to posterior parietal area 7 regions is provided in Fig. 8. It should be noted that the area 5 regions in humans appear to be displaced dorsally with respect to their location in macaques such that the area 5 regions roll over to the medial wall of the hemispheres (Fig. 8). In Fig. 8 (based on the data in Figs. 2–4), the connectivity from the primary somatosensory cortex area 3b partly via areas 1 and 2 to area 5 somatosensory regions 5m > 5L > 5mv is shown with green arrows. The onward connectivity of 5mv to for example posterior parietal 7AL, 7Am, and 7PC which have connectivity with intraparietal regions, such as LIP, is shown with red arrows. The pathway in more detail is as follows, where > reflects an effective connectivity but does not exclude effects across levels:

$$(3b + 3a <> 1 + 2) <> 5m <> 5L <> 5mv <> 7AL, 7Am \text{ and } 7PC.$$

5mv also has connectivity to 6mp, TPOJ2, and the supracallosal anterior cingulate cortex p32pr, a32pr, and a24pr.

Given that area 7 is involved in actions in space (Andersen 1995; Snyder et al. 1998; Dean and Platt 2006; Vedder et al. 2017; Avila et al. 2019; Gamberini et al. 2020; Rolls 2020b; Orban et al. 2021; Passarelli et al. 2021; Rolls 2021a; Rolls, Deco, et al. 2022b), this dorsal somatosensory stream may be characterized as an "action" "where" stream.

Another feature of the connectivity shown in Figs. 2–4 is that the somatosensory cortical areas do have connectivity directed toward motor (area 4), premotor (area 6), or midcingulate premotor cortex. This is a principle established in macaques (Rizzolatti and Sinigaglia 2016) and presumably allows appropriate movements to be made to the somatosensory/proprioceptive properties analyzed in each somatosensory/proprioceptive region.

Taste cortical regions

AVI and FOP3-5 are where in the HCP-MMP atlas the human primary taste cortex is located in the anterior dorsal (i.e. superior) insula and adjoining frontal operculum (Rolls 2015, 2016a, 2016c). The taste inputs to these regions are received from the thalamus ventro-postero-medial nucleus pars parvocellularis (Pritchard et al. 1986; Norgren 1990). In primates, it has been discovered that neurons in the primary taste cortex (in the rostro-dorsal insula and adjoining frontal operculum) have responses to the 5 primary taste stimuli sweet, salt, bitter, sour, and glutamate (umami) (Scott et al. 1986; Yaxley et al. 1990; Baylis and Rolls 1991; Rolls et al. 1996), with each neuron having a different profile of responses to this set of stimuli and thereby having information that increases approximately linearly with the number of neurons (Kadohisa et al. 2005; Rolls et al. 2010; Rolls and Treves 2011). The primary taste cortex in macaques has onward connections to the orbitofrontal cortex (Baylis et al. 1995), and in this secondary taste cortical area, neurons have also been discovered that respond to taste (Rolls et al. 1990). In the primary taste cortex, feeding to

satiety does not reduce the responses of neurons to the taste of the food eaten to satiety, providing evidence that the primary taste cortex represents "what" the taste is, independently of its reward value (Rolls et al. 1988; Yaxley et al. 1988). By contrast, in the orbitofrontal cortex, the responses of neurons decrease to zero to the food eaten to satiety, providing evidence that the reward value of the taste is represented in the orbitofrontal cortex (Rolls et al. 1989). A similar situation appears to hold in humans in that feeding to satiety decreases orbitofrontal cortex activations to the food eaten to satiety (Kringelbach et al. 2003), and the orbitofrontal cortex BOLD signal is correlated with the pleasantness of the taste, whereas in the insular taste cortex, the BOLD signal is correlated with the intensity of the taste and not with its pleasantness (Grabenhorst and Rolls 2008).

However, the taste cortex is even more interesting than this, for it also represents the texture of food, which is a signal of somatosensory origin, in that some macaque neurons in the insula primary taste cortex respond to viscosity, others to rough texture, and others to the texture of fat in the mouth with responses related to the coefficient of sliding friction (Verhagen et al. 2004), which is how we have discovered fat in the mouth is sensed (Rolls 2016c; Rolls et al. 2018), with similar encoding of texture as well as taste in the orbitofrontal cortex (Verhagen et al. 2003). A similar situation appears to hold in humans in that the BOLD signal in the taste cortical areas can also be related to viscosity; and in some regions, there is evidence that fat texture is represented (Kringelbach et al. 2003; de Araujo and Rolls 2004; Grabenhorst et al. 2010). Part of the interest of the present investigation is that it shows how the insular and FOP regions do receive somatosensory inputs (Figs. 2–4), which are needed if responses are to be found to oral texture stimuli such as viscosity, roughness, and fat texture (Rolls 2020a). These discoveries, including that fat texture is sensed by the coefficient of sliding friction (Rolls et al. 2018), help to provide a foundation for understanding the roles of the sensory qualities of food in the control of appetite and food intake (Rolls 2016c, 2016d, 2018a).

Motor and premotor frontal cortical regions

Helpful descriptions of the connectivity of motor and premotor cortical regions and their inputs from intraparietal sulcus and inferior parietal cortex regions for macaques have been provided elsewhere (Rizzolatti and Kalaska 2013; Rizzolatti and Sinigaglia 2016; Gerbella et al. 2017). In this paper, the connectivity of these motor and premotor areas with other cortical regions is extended to humans and in particular to cortical regions as defined in the HCP-MMP atlas (Glasser, Coalson, et al. 2016a). Highlights of the present results are that the area 6 regions have connectivity not only from postcentral somatosensory cortical regions, such as 1, 2, 3 and 5, but also from parts of parietal area 7 and from the intraparietal regions (Rolls, Deco, et al. 2022b). The inputs from the latter two parietal systems are likely to be important in functions such as visually guided actions in space (Rizzolatti and Kalaska 2013; Rizzolatti and Sinigaglia 2016; Fattori et al. 2017; Gerbella et al. 2017; Gamberini et al. 2020). The area 6 regions also receive from the midcingulate premotor regions (24dd, 24dv, and 23c), which receiving from the supracallosal anterior cingulate cortex provide a route for action-outcome learning and performance (Rolls 2022b; Rolls, Deco, et al. 2022f).

Inferior frontal gyrus (regions 44, 45, 47l, a47r, IFJa, IFJp, IFSa, IFSp, and p47r)

The three inferior frontal gyrus regions 44, 45, and 47l are considered briefly first, as they have been considered previously in an investigation of the human language connectome (Rolls, Deco, et al. 2022d). Areas 44 and 45 are brain regions normally considered as Broca's area (Petrides 2014; Friederici et al. 2017; Rauschecker 2018; Milton et al. 2021; Weiller et al. 2021; Sprung-Much et al. 2022), but 47l at least in the left hemisphere has very similar connectivity to them. These regions receive from two semantic systems. One semantic system is in the ventral part of the STS (STSva and STSvp) connected with the inferior temporal visual cortical TE regions and parietal PGi and PGs involved in the visual representations of objects (Rolls, Deco, et al. 2022d). A second semantic system is in the STSda and STSdp, STGa, auditory A5, TPOJ1, the STV, and the PSL and has effective connectivity with auditory areas (A1, A4, A5, and Pbelt); with relatively early visual areas involved in motion, e.g. MT and MST, and faces/words, e.g. FFC; with somatosensory regions (frontal opercular FOP, insula, and parietal PF); with other TPOJ regions; and with the inferior frontal gyrus regions (IFJa and IFSp) (Rolls, Deco, et al. 2022d). In macaques, area 45 has connectivity with the cortex in the STS (Petrides and Pandya 2002). Of especial relevance to the findings described here, the somatosensory "ventral what stream" regions (FOP, insula, and parietal PF) are incorporated into the second semantic system (Rolls, Deco, et al. 2022d), and the somatosensory "dorsal action" stream is less incorporated into language-related semantic processing. Also of especial interest is that Broca's area 44 and 45 at least in the left hemisphere involves much surrounding cortex as shown by the connectivity, including 47l which is part of the lateral orbitofrontal cortex, and whole swathes of the inferior frontal gyrus, including IFJa and IFsp and IFsa which are strongly interconnected (Figs. 2 and 3). Area 44 is implicated in syntax (Friederici et al. 2017), but the close interconnections of 44, 45 47l, IFJa, IFsp, and IFsa are consistent with the hypothesis that inferior frontal gyrus sequentially linked attractor networks could provide an implementation of the sequential syntactic operations involved in speech production, but would need many such linked attractor systems to deal with the different sequential processing needed for the active versus the passive tense, and for different languages (Rolls and Deco 2015).

The connectivity of inferior frontal regions IFJa, IFJp, IFSa, and IFSp is considered next, with Fig. 9 providing a schematic overview of the effective connectivity of IFSa, chosen as typical of this set of interconnected regions. A feature of the connectivity of the IFJ and IFS regions are that they receive from inferior temporal visual cortical regions (e.g. TE1p, TE2a, TE2p, and PHT, see Fig. 2) involved in object representations (Rolls 2021d, 2021c; Rolls, Deco, et al. 2022a). This makes it likely that in humans these IFJ and IFS regions specialize in the short-term memory of visual object-based "what" representations. The connectivity of some of these regions with language-related regions 44, 45, 47l, TPOJ1, STV, 55b, and some STS regions also provide a route for this visual object- and face-related information to gain access to these language-related regions (Rolls, Deco, et al. 2022d). There are also some inputs from intraparietal visual motion-/grasp-related regions (Rolls, Deco, et al. 2022b), such as AIP, LIPd, MIP, and IP0-2, so that some aspects of the motion of objects, also represented in the STS regions (Rolls, Deco, et al. 2022a), are utilized in the inferior frontal regions. Interestingly, there are also inputs from the orbitofrontal cortex (e.g. 11l and 13l) involved in reward/punishment value representations and thereby in emotion (Rolls 2019a, 2019b; Rolls, Deco, et al. 2022f) (Fig. 2, see Results section). The IFS and IFJ regions may therefore be involved in maintaining information about visual objects, visual motion, and emotional value and mood in short-term memory by maintaining firing in attractor networks in these inferior frontal gyrus regions

(Martinez-Garcia et al. 2011; Fuster 2015; Constantinidis et al. 2018; Rolls 2021c). These IFS and IFJ regions also provide a route for these types of input to access language systems and may also provide additional attractor networks that can be involved with Broca's area regions in syntax (Rolls and Deco 2015; Rolls, Deco, et al. 2022d).

a47r and p47r are the anterolateral parts of the orbitofrontal cortex (Fig. 1) considered elsewhere (Rolls, Deco, et al. 2022f). They have connectivity with other orbitofrontal cortex regions (13l, 11l, OFC, and 47m), inferior temporal cortex (TE1p, TE2a, TE1m, and PHT), medial prefrontal 8BM, and PFm (Fig. 2) and are involved in value-/emotion-related processing (Rolls 2019a, 2019b; Rolls et al. 2020; Rolls, Deco, et al. 2022f).

Dorsolateral prefrontal cortex division (46, 8Ad, 8Av, 8BL, 8C, 9-46d, 9a, 9p, a9-46v, i6-8, p9-46v, and s6-8)

A first group of regions comprises DLPFC regions 46, 9-46d, a9-46v, and p9-46v, with the connectivity of region 46 a key example illustrated schematically in Fig. 10. These regions have connectivity with superior parietal cortex regions in area 7 and intraparietal regions involved in actions in space ("where") and with inferior parietal PF and PFm and the insula which can be considered as in the somatosensory "what" hierarchy as described above (Fig. 2) (Rolls, Deco, et al. 2022b). Interestingly, these regions also receive inputs from the orbitofrontal cortex (11l and 13l, Figs. 2 and 10). These regions are thus classic DLPFC regions and are probably involved in limb-/body-related spatial working memory functions probably in egocentric space (rather than eye movement-related) (Passingham 2021). There is connectivity directed toward premotor 6ma, 6a, and 6r and the midcingulate motor region 23c and to the supracallosal anterior cingulate a24pr, p24pr, a32pr, p32pr, and 33pr. The latter connectivity could be useful it is proposed for action-outcome learning implemented in the supracallosal anterior cingulate cortex (Rolls, Deco, et al. 2022f) by providing a memory-related input about recent actions until a reward or punishment outcome is received.

A second group of regions that is more dorsal (superior) in the prefrontal cortex comprises 8Ad, 8Av, 8BL, 9p, i6-8, and s6-8, with the connectivity of region 8Ad as an example illustrated schematically in Fig. 11. The effective connectivity of this "dorsal prefrontal" group with the inferior parietal visual regions PFm, PGs, and PGi is notable. There is also connectivity with the entorhinal cortex (EC) and parahippocampal gyrus regions PHA1-2 and with the memory-related parts of the posterior cingulate division (31pd, 31pv, and v23ab) and 7m (Rolls, Wirth, et al. 2022h). This group also has some connectivity with visual inferior temporal TE1m, TE1p, and TE2a; and with STSvp; and with the frontal pole a10p and p10p. Regions 8BL, 9a, and 9p have connectivity with temporal pole TGd and TGv. Region 8Ad also has some connectivity with reward-related regions the ventromedial prefrontal cortex 10d and 10r and the pregenual anterior cingulate cortex d32 and p32 (Rolls, Deco, et al. 2022f). Region 8Ad has moderate effective connectivity with other dorsal prefrontal regions 8Av, 9p, i6-8, and s6-8. There is connectivity directed toward language regions, the SFL, 44, 45, 47l, and 55b, and to the premotor eye field PEF. These dorsal frontal regions in front of the eye fields may be involved in visual and auditory attention (Germann and Petrides 2020a, 2020b; Passingham 2021), and their connectivity with inferior parietal visual/multimodal cortical regions may be part of the implementation of top-down attention (Deco and Rolls 2005a; Deco and Rolls 2005b; Rolls 2021c).

The computational functions of these dorsolateral and dorsal prefrontal cortex regions are likely to be to maintain information in short-term/working memory by maintaining firing in attractor networks (Funahashi et al. 1989; Goldman-Rakic 1996; Martinez–Garcia et al. 2011; Fuster 2015; Constantinidis et al. 2018; Rolls 2021c). The DLPFC could thereby implement some aspects of executive function (Funahashi 2017), with those aspects perhaps being described better not as "voluntary action" (Passingham and Wise 2012; Passingham 2021), which is difficult to define and measure, but instead as "internally generated from for example memory." But other key aspects of the dorsolateral and dorsal prefrontal cortex include top-down attention implemented by providing the biasing source held in short-term memory, which can also bias action selection (Deco and Rolls 2003; Deco and Rolls 2004, 2005a; Rolls 2021c). Another key property of prefrontal cortex attractor networks may be not only holding information in a short-term memory but also transferring information using linked attractor networks from, for example, a short-term memory attractor network for sensory stimuli to another attractor network in which actions are represented (Deco et al. 2005), thereby implementing stimulus-delay-response tasks.

In macaques, the connections and neuronal recordings suggest the following subregions of the DLPFC (Petrides and Pandya 1999; Kelly et al. 2010; Petrides et al. 2012; Yeterian et al. 2012; Petrides 2014; Pandya et al. 2015; Goulas et al. 2017; Passingham 2021). The posterior part near the arcuate sulcus contains a frontal eye field FEF. A dorsal part, FEFd is closely associated with the immediately anterior 8Ad, which has connectivity with dorsal stream intraparietal regions, and a ventral part FEFv is closely associated with the immediately anterior 8Av which has connectivity with ventral stream inferior temporal visual cortex regions (Petrides and Pandya 1999; Passingham 2021). The FEF and the adjacent area 46 cortex in the posterior part of the principal sulcus is especially implicated in eye movements to visual stimuli remembered over a short delay (Funahashi et al. 1989, 1993; Goldman-Rakic 1996), which is consistent with short-term memory functions of the dorsolateral prefrontal regions. The more mid- and anterior parts of area 46 in the macaque principal sulcus are involved more in remembered limb movements (Passingham 2021). In humans, area 46 is far anterior (Sallet et al. 2013) and probably includes some of 46 and a9-46v in the HCP-MMP atlas (Glasser, Coalson, et al. 2016a; Huang et al. 2022) (Fig. 1).

The use of effective connectivity

Effective connectivity is helpful in enabling estimation of the connectivity in each direction between every pair of brain regions and is consistent with causal effects. Effective connectivity thus helps us to build hypotheses about how information flows through the system, and that is helpful, when complemented with evidence about what is represented in each brain region and the effects of damage to each brain region, in building a model of how the brain works computationally (Rolls 2021c). This helps in understanding the serial nature of information processing in some of the sensory cortical hierarchies (Rolls 2021c), including the somatosensory cortical hierarchy described here that reaches inferior parietal PF. However, at the same time, the effective connectivity makes it clear that in most cases there is at least some connectivity in the opposite direction, and the utility of this for processes such as memory recall and top-down attention is starting to be understood computationally (Treves and Rolls 1994; Deco and Rolls 2005a; Rolls 2016b, 2018b, 2021c, 2022b). It must also be understood that there is considerable selectivity of the connectivity, with the mean sparseness of the connectivity 0.11

(meaning that on average any one cortical region makes connections with only about 11% of other cortical regions, with the selectivity greater than this when it is recognized that the number of strong connectivities is much smaller than this) in this series of papers (Rolls, Deco, et al., 2022a, 2022b, 2022c, 2022d, 2022e, 2022f; Rolls, Rauschecker, et al. 2022g; Rolls, Wirth, et al. 2022h). The implication of this is that different sensory cortical systems can operate relatively independently of each other in their early stages of the hierarchy and can then be brought together with signals from other hierarchies after several stages to form multimodal representations that lead eventually to semantic representations (Rolls 2021c; Rolls, Deco, et al. 2022a, 2022d).

Conclusions

The research described here, in which an effective connectivity algorithm was used in conjunction with the HCP-MMP (Glasser, Coalson, et al. 2016a; Huang et al. 2022) and HCP data at 7T (Smith et al. 2013; Glasser, Smith, et al. 2016b), leads to the following advances in our understanding of the human frontal lobes, somatosensory cortex, and insula.

A ventral somatosensory stream connects from areas 3b and 3a via area 1 and area 2 and then via opercular and frontal opercular regions to the insula which then connects to inferior parietal PF regions. This stream is implicated in "what" related somatosensory processing of objects and of the body and in combining with visual inputs in PF to form multimodal representations. This system is important in forming representations of one's own body and in feeling ownership of it. Part of this system includes the primary taste cortex in anterior insular AVI and FOP cortex FOP3-5, which provides representations of "what" taste and texture is present in the mouth (Rolls 2015, 2016c, 2016a; Rolls et al. 2018).

A dorsal action somatosensory stream connects from areas 3b and 3a via areas 1 and 2 to parietal area 5 and then 7. This stream is important in actions in space, including, for example, reaching toward and grasping an object.

Inferior prefrontal regions (IFS and IFG) have connectivity with the inferior temporal visual cortex and orbitofrontal cortex and are connected with language systems, including 44, 45, 47l, TPOJ1, and STV. These inferior prefrontal regions are implicated in working memory for "what" processing streams and in linking with language regions 44 and 45 for which they may provide extra attractor short-term memory system for use in syntax.

The DLPFC regions that include area 46 have connectivity with parietal area 7 and somatosensory PFs and are implicated in working memory for actions; and in humans, they provide the basis for linked steps of plans with each step held in working memory.

The dorsal prefrontal regions that include 8Ad and 8Av have connectivity with the visual regions of the inferior parietal cortex, including PGs and PGi, and also with the hippocampal system and memory-related parts of the posterior cingulate cortex and are implicated in visual attention which requires a short-term memory to maintain the top-down bias for biased competition (Deco and Rolls 2005a; Deco and Rolls 2005b; Rolls 2021c).

Acknowledgements

The neuroimaging data were provided by the HCP, WU-Minn Consortium (Principal Investigators: David Van Essen and Kamil Ugurbil; 1U54MH091657) funded by the 16 NIH Institutes and Centers that support the NIH Blueprint for Neuroscience Research; and by the McDonnell Center for Systems Neuroscience at Washington University. Dr Wei Cheng and Shitong Xiang of ISTBI, Fudan University, Shanghai are thanked for parcellating the data into HCP-MMP surface-based space (Glasser, Coalson, et al. 2016a) and reordering it into HCPex order (Huang et al. 2022). Roscoe Hunter of the University of Warwick is thanked for contributing to the description in the Supplementary Material of the Hopf effective connectivity algorithm.

Supplementary material

Supplementary material is available at *Cerebral Cortex* online.

Funding

The work was supported by the following grants. Professor J. Feng: National Key R&D Program of China (No. 2019YFA0709502); 111 Project (No. B18015); Shanghai Municipal Science and Technology Major Project (No. 2018SHZDZX01), ZJLab, and Shanghai Center for Brain Science and Brain-Inspired Technology; and National Key R&D Program of China (No. 2018YFC1312904). GD is supported by a Spanish national research project (ref. PID2019-105772GB-I00 MCIU AEI) funded by the Spanish Ministry of Science, Innovation and Universities (MCIU), State Research Agency (AEI); HBP SGA3 Human Brain Project Specific Grant Agreement 3 (grant agreement no. 945539), funded by the EU H2020 FET Flagship programme; SGR Research Support Group support (ref. 2017 SGR 1545), funded by the Catalan Agency for Management of University and Research Grants (AGAUR); Neurotwin Digital twins for model-driven non-invasive electrical brain stimulation (grant agreement ID: 101017716) funded by the EU H2020 FET Proactive programme; euSNN European School of Network Neuroscience (grant agreement ID: 860563) funded by the EU H2020 MSCA-ITN Innovative Training Networks; CECH The Emerging Human Brain Cluster (Id. 001-P-001682) within the framework of the European Research Development Fund Operational Program of Catalonia 2014–2020; Brain-Connects: Brain Connectivity during Stroke Recovery and Rehabilitation (id. 201725.33) funded by the Fundacio La Marato TV3; Corticity, FLAG¨ERA JTC 2017, (ref. PCI2018-092891) funded by the Spanish Ministry of Science, Innovation and Universities (MCIU), State Research Agency (AEI). The funding sources had no role in the study design; in the collection, analysis and interpretation of data; in the writing of the report; and in the decision to submit the article for publication.

Conflict of interest statement: None declared.

Data and code availability

The data are available at the HCP website http://www.humanconnectome.org/. Code for the Hopf effective connectivity algorithm is available at https://github.com/decolab/Effective-Connectivity--Hopf.

Authors' contributions

Edmund T. Rolls designed and performed the research and wrote the paper. Gustavo Deco provided the effective connectivity algorithm. Chu-Chung Huang performed the diffusion tractography and prepared the brain figures with the HCP-MMP labels. Jianfeng Feng performed the funding acquisition. All authors approved the paper.

Ethical permissions

No data were collected as part of the research described here. The data were from the HCP, and the WU-Minn HCP Consortium obtained full informed consent from all participants, and research procedures and ethical guidelines were followed in accordance with the Institutional Review Boards, with details at the HCP website http://www.humanconnectome.org/

References

Andersen RA. Encoding of intention and spatial location in the posterior parietal cortex. *Cereb Cortex*. 1995:5(5):457–469.

Avila E, Lakshminarasimhan KJ, DeAngelis GC, Angelaki DE. Visual and vestibular selectivity for self-motion in macaque posterior parietal area 7a. *Cereb Cortex*. 2019:29(9):3932–3947.

Bajaj S, Adhikari BM, Friston KJ, Dhamala M. Bridging the gap: dynamic causal modeling and granger causality analysis of resting state functional magnetic resonance imaging. *Brain Connect*. 2016:6(8):652–661.

Baker CM, Burks JD, Briggs RG, Conner AK, Glenn CA, Morgan JP, Stafford J, Sali G, McCoy TM, Battiste JD, et al. A connectomic atlas of the human cerebrum-chapter 2: the lateral frontal lobe. *Oper Neurosurg (Hagerstown)*. 2018a:15(suppl_1):S10–S74.

Baker CM, Burks JD, Briggs RG, Conner AK, Glenn CA, Robbins JM, Sheets JR, Sali G, McCoy TM, Battiste JD, et al. A connectomic atlas of the human cerebrum-chapter 5: the insula and opercular cortex. *Oper Neurosurg (Hagerstown)*. 2018b:15(suppl_1):S175–S244.

Baker CM, Burks JD, Briggs RG, Conner AK, Glenn CA, Taylor KN, Sali G, McCoy TM, Battiste JD, O'Donoghue DL, et al. A connectomic atlas of the human cerebrum-chapter 7: the lateral parietal lobe. *Oper Neurosurg (Hagerstown)*. 2018c:15(suppl_1):S295–S349.

Baker CM, Burks JD, Briggs RG, Milton CK, Conner AK, Glenn CA, Sali G, McCoy TM, Battiste JD, O'Donoghue DL, et al. A connectomic atlas of the human cerebrum-chapter 6: the temporal lobe. *Oper Neurosurg (Hagerstown)*. 2018d:15(suppl_1):S245–S294.

Baker CM, Burks JD, Briggs RG, Sheets JR, Conner AK, Glenn CA, Sali G, McCoy TM, Battiste JD, O'Donoghue DL, et al. A connectomic atlas of the human cerebrum-chapter 3: the motor, premotor, and sensory cortices. *Oper Neurosurg (Hagerstown)*. 2018e:15(suppl_1):S75–S121.

Baylis LL, Rolls ET. Responses of neurons in the primate taste cortex to glutamate. *Physiol Behav*. 1991:49(5):973–979.

Baylis LL, Rolls ET, Baylis GC. Afferent connections of the caudolateral orbitofrontal cortex taste area of the primate. *Neuroscience*. 1995:64(3):801–812.

Catani M, Thiebaut de Schotten M. A diffusion tensor imaging tractography atlas for virtual in vivo dissections. *Cortex*. 2008:44(8):1105–1132.

Colclough GL, Smith SM, Nichols TE, Winkler AM, Sotiropoulos SN, Glasser MF, Van Essen DC, Woolrich MW. The heritability of multi-modal connectivity in human brain activity. *Elife*. 2017:6:e20178.

Constantinidis C, Funahashi S, Lee D, Murray JD, Qi XL, Wang M, Arnsten AFT. Persistent spiking activity underlies working memory. *J Neurosci*. 2018:38(32):7020–7028.

Craig AD. How do you feel—now? The anterior insula and human awareness. *Nat Rev Neurosci*. 2009:10(1):59–70.

Craig AD. Significance of the insula for the evolution of human awareness of feelings from the body. *Ann N Y Acad Sci*. 2011:1225(1):72–82.

de Araujo IET, Rolls ET. The representation in the human brain of food texture and oral fat. *J Neurosci*. 2004:24(12):3086–3093.

de Haan EHF, Dijkerman HC. Somatosensation in the brain: a theoretical re-evaluation and a new model. *Trends Cogn Sci*. 2020:24(7):529–541.

Dean HL, Platt ML. Allocentric spatial referencing of neuronal activity in macaque posterior cingulate cortex. *J Neurosci*. 2006:26(4):1117–1127.

Deco G, Rolls ET. Attention and working memory: a dynamical model of neuronal activity in the prefrontal cortex. *Eur J Neurosci*. 2003:18(8):2374–2390.

Deco G, Rolls ET. A neurodynamical cortical model of visual attention and invariant object recognition. *Vis Res*. 2004:44(6):621–642.

Deco G, Rolls ET. Attention, short-term memory, and action selection: a unifying theory. *Prog Neurobiol*. 2005a:76(4):236–256.

Deco G, Rolls ET. Neurodynamics of biased competition and cooperation for attention: a model with spiking neurons. *J Neurophysiol*. 2005b:94(1):295–313.

Deco G, Ledberg A, Almeida R, Fuster J. Neural dynamics of cross-modal and cross-temporal associations. *Exp Brain Res*. 2005:166(3–4):325–336.

Deco G, Cabral J, Woolrich MW, Stevner ABA, van Hartevelt TJ, Kringelbach ML. Single or multiple frequency generators in on-going brain activity: a mechanistic whole-brain model of empirical MEG data. *NeuroImage*. 2017a:152:538–550.

Deco G, Kringelbach ML, Jirsa VK, Ritter P. The dynamics of resting fluctuations in the brain: metastability and its dynamical cortical core. *Sci Rep*. 2017b:7(1):3095.

Deco G, Cruzat J, Cabral J, Tagliazucchi E, Laufs H, Logothetis NK, Kringelbach ML. Awakening: predicting external stimulation to force transitions between different brain states. *Proc Natl Acad Sci*. 2019:116(36):18088–18097.

Delhaye BP, Long KH, Bensmaia SJ. Neural basis of touch and proprioception in primate cortex. *Compr Physiol*. 2018:8(4):1575–1602.

Dhollander T, Raffelt D, Connelly A. 2016. Unsupervised 3-tissue response function estimation from single-shell or multi-shell diffusion MR data without a co-registered T1 image. *ISMRM Workshop on Breaking the Barriers of Diffusion MRI* 5.

Fattori P, Breveglieri R, Bosco A, Gamberini M, Galletti C. Vision for prehension in the medial parietal cortex. *Cereb Cortex*. 2017:27(2):1149–1163.

Frassle S, Lomakina EI, Razi A, Friston KJ, Buhmann JM, Stephan KE. Regression DCM for fMRI. *NeuroImage*. 2017:155:406–421.

Freyer F, Roberts JA, Becker R, Robinson PA, Ritter P, Breakspear M. Biophysical mechanisms of multistability in resting-state cortical rhythms. *J Neurosci*. 2011:31(17):6353–6361.

Freyer F, Roberts JA, Ritter P, Breakspear M. A canonical model of multistability and scale-invariance in biological systems. *PLoS Comput Biol*. 2012:8(8):e1002634.

Friederici AD, Chomsky N, Berwick RC, Moro A, Bolhuis JJ. Language, mind and brain. *Nat Hum Behav*. 2017:1(10):713–722.

Friston K. Causal modelling and brain connectivity in functional magnetic resonance imaging. *PLoS Biol*. 2009:7(2):e33.

Funahashi S. Working memory in the prefrontal cortex. *Brain Sci*. 2017:7(12):49.

Funahashi S, Bruce CJ, Goldman-Rakic PS. Mnemonic coding of visual space in monkey dorsolateral prefrontal cortex. *J Neurophysiol*. 1989:61(2):331–349.

Funahashi S, Bruce CJ, Goldman-Rakic PS. Dorsolateral prefrontal lesions and oculomotor delayed-response performance: evidence for mnemonic "scotomas". *J Neurosci*. 1993:13(4):1479–1497.

Fuster JM. *The prefrontal cortex*. London: Academic Press; 2015.

Fuster JM. Cognitive networks (Cognits) process and maintain working memory. *Front Neural Circuits*. 2021:15:790691.

Gamberini M, Passarelli L, Fattori P, Galletti C. Structural connectivity and functional properties of the macaque superior parietal lobule. *Brain Struct Funct*. 2020:225(4):1349–1367.

Gardner EP. Dorsal and ventral streams in the sense of touch. In: *The senses: a comprehensive reference*. New York: Academic Press; 2008. pp. 233–258

Gerbella M, Rozzi S, Rizzolatti G. The extended object-grasping network. *Exp Brain Res*. 2017:235(10):2903–2916.

Germann J, Petrides M. Area 8A within the posterior middle frontal gyrus underlies cognitive selection between competing visual targets. *eNeuro*. 2020a:7(5):ENEURO.0102–ENEU20.2020.

Germann J, Petrides M. The ventral part of dorsolateral frontal area 8A regulates visual attentional selection and the dorsal part auditory attentional selection. *Neuroscience*. 2020b:441:209–216.

Gilson M, Moreno-Bote R, Ponce-Alvarez A, Ritter P, Deco G. Estimation of directed effective connectivity from fMRI functional connectivity hints at asymmetries in the cortical connectome. *PLoS Comput Biol*. 2016:12(3):e1004762.

Glasser MF, Sotiropoulos SN, Wilson JA, Coalson TS, Fischl B, Andersson JL, Xu J, Jbabdi S, Webster M, Polimeni JR, et al. The minimal preprocessing pipelines for the human connectome project. *NeuroImage*. 2013:80:105–124.

Glasser MF, Coalson TS, Robinson EC, Hacker CD, Harwell J, Yacoub E, Ugurbil K, Andersson J, Beckmann CF, Jenkinson M, et al. A multi-modal parcellation of human cerebral cortex. *Nature*. 2016a:536(7615):171–178.

Glasser MF, Smith SM, Marcus DS, Andersson JL, Auerbach EJ, Behrens TE, Coalson TS, Harms MP, Jenkinson M, Moeller S, et al. The human connectome Project's neuroimaging approach. *Nat Neurosci*. 2016b:19(9):1175–1187.

Goldman-Rakic PS. The prefrontal landscape: implications of functional architecture for understanding human mentation and the central executive. *Philos Trans R Soc B*. 1996:351(1346):1445–1453.

Goldman-Rakic PS, Leung H-C. Functional architecture of the dorsolateral prefrontal cortex in monkeys and humans. In: Stuss DT, Knight RT, editors. *Principles of frontal lobe function*. New York: Oxford University Press; 2002. pp. 85–95

Goodale MA, Milner AD. Separate visual pathways for perception and action. *Trends Neurosci*. 1992:15(1):20–25.

Goulas A, Stiers P, Hutchison RM, Everling S, Petrides M, Margulies DS. Intrinsic functional architecture of the macaque dorsal and ventral lateral frontal cortex. *J Neurophysiol*. 2017:117(3):1084–1099.

Grabenhorst F, Rolls ET. Selective attention to affective value alters how the brain processes taste stimuli. *Eur J Neurosci*. 2008:27(3):723–729.

Grabenhorst F, Rolls ET. Value, pleasure, and choice in the ventral prefrontal cortex. *Trends Cogn Sci*. 2011:15(2):56–67.

Grabenhorst F, Rolls ET, Parris BA, D'Souza A. How the brain represents the reward value of fat in the mouth. *Cereb Cortex*. 2010:20(5):1082–1091.

Griffanti L, Salimi-Khorshidi G, Beckmann CF, Auerbach EJ, Douaud G, Sexton CE, Zsoldos E, Ebmeier KP, Filippini N, Mackay CE, et al. ICA-based artefact removal and accelerated fMRI acquisition for improved resting state network imaging. *NeuroImage*. 2014:95:232–247.

Huang C-C, Rolls ET, Hsu C-CH, Feng J, Lin C-P. Extensive cortical connectivity of the human hippocampal memory system: beyond the "what" and "where" dual-stream model. *Cereb Cortex*. 2021:31(10):4652–4669.

Huang CC, Rolls ET, Feng J, Lin CP. An extended human connectome project multimodal parcellation atlas of the human cortex and subcortical areas. *Brain Struct Funct*. 2022:227(3):763–778.

Jeurissen B, Tournier JD, Dhollander T, Connelly A, Sijbers J. Multi-tissue constrained spherical deconvolution for improved analysis of multi-shell diffusion MRI data. *NeuroImage*. 2014:103:411–426.

Kadohisa M, Rolls ET, Verhagen JV. Neuronal representations of stimuli in the mouth: the primate insular taste cortex, orbitofrontal cortex, and amygdala. *Chem Senses*. 2005:30(5):401–419.

Kelly C, Uddin LQ, Shehzad Z, Margulies DS, Castellanos FX, Milham MP, Petrides M. Broca's region: linking human brain functional connectivity data and non-human primate tracing anatomy studies. *Eur J Neurosci*. 2010:32(3):383–398.

Kringelbach ML, Deco G. Brain states and transitions: insights from computational neuroscience. *Cell Rep*. 2020:32(10):108128.

Kringelbach ML, O'Doherty J, Rolls ET, Andrews C. Activation of the human orbitofrontal cortex to a liquid food stimulus is correlated with its subjective pleasantness. *Cereb Cortex*. 2003:13(10):1064–1071.

Kringelbach ML, McIntosh AR, Ritter P, Jirsa VK, Deco G. The rediscovery of slowness: exploring the timing of cognition. *Trends Cogn Sci*. 2015:19(10):616–628.

Kuznetsov YA. *Elements of applied bifurcation theory*. New York: Springer Science & Business Media; 2013

Ma Q, Rolls ET, Huang C-C, Cheng W, Feng J. Extensive cortical functional connectivity of the human hippocampal memory system. *Cortex*. 2022:147:83–101.

Maier-Hein KH, Neher PF, Houde JC, Cote MA, Garyfallidis E, Zhong J, Chamberland M, Yeh FC, Lin YC, Ji Q, et al. The challenge of mapping the human connectome based on diffusion tractography. *Nat Commun*. 2017:8(1):1349.

Martinez-Garcia M, Rolls ET, Deco G, Romo R. Neural and computational mechanisms of postponed decisions. *Proc Natl Acad Sci U S A*. 2011:108(28):11626–11631.

McCabe C, Rolls ET, Bilderbeck A, McGlone F. Cognitive influences on the affective representation of touch and the sight of touch in the human brain. *Soc Cogn Affect Neurosci*. 2008:3(2):97–108.

Milner AD, Goodale MA. *The visual brain in action*. Oxford: Oxford University Press; 1995

Milton CK, Dhanaraj V, Young IM, Taylor HM, Nicholas PJ, Briggs RG, Bai MY, Fonseka RD, Hormovas J, Lin YH, et al. Parcellation-based anatomic model of the semantic network. *Brain Behav*. 2021:11(4):e02065.

Mishkin M. Analogous neural models for tactual and visual learning. *Neuropsychologia*. 1979:17(2):139–151.

Norgren R. Gustatory system. In: Paxinos G, editors. *The human nervous system*. San Diego: Academic; 1990. pp. 845–861

O'Connor DH, Krubitzer L, Bensmaia S. Of mice and monkeys: somatosensory processing in two prominent animal models. *Prog Neurobiol*. 2021:201:102008.

Orban GA, Sepe A, Bonini L. Parietal maps of visual signals for bodily action planning. *Brain Struct Funct*. 2021:226(9):2967–2988.

Pandya DN, Seltzer B, Petrides M, Cipolloni PB. *Cerebral cortex: architecture, connections, and the dual origin concept*. New York: Oxford University Press; 2015.

Passarelli L, Gamberini M, Fattori P. The superior parietal lobule of primates: a sensory-motor hub for interaction with the environment. *J Integr Neurosci*. 2021:20(1):157–171.

Passingham RE. *Understanding the prefrontal cortex: selective advantage, connectivity and neural operations*. Oxford: Oxford University Press; 2021.

Passingham REP, Wise SP. *The neurobiology of the prefrontal cortex*. Oxford: Oxford University Press; 2012.

Petrides M. *Neuroanatomy of language regions of the human brain*. New York: Academic Press; 2014.

Petrides M, Pandya DN. Dorsolateral prefrontal cortex: comparative cytoarchitectonic analysis in the human and the macaque brain and corticocortical connection patterns. *Eur J Neurosci*. 1999:11(3):1011–1036.

Petrides M, Pandya DN. Comparative cytoarchitectonic analysis of the human and the macaque ventrolateral prefrontal cortex and corticocortical connection patterns in the monkey. *Eur J Neurosci*. 2002:16(2):291–310.

Petrides M, Tomaiuolo F, Yeterian EH, Pandya DN. The prefrontal cortex: comparative architectonic organization in the human and the macaque monkey brains. *Cortex*. 2012:48(1):46–57.

Power JD, Cohen AL, Nelson SM, Wig GS, Barnes KA, Church JA, Vogel AC, Laumann TO, Miezin FM, Schlaggar BL, et al. Functional network organization of the human brain. *Neuron*. 2011:72(4):665–678.

Pritchard TC, Hamilton RB, Morse JR, Norgren R. Projections of thalamic gustatory and lingual areas in the monkey, *Macaca fascicularis*. *J Comp Neurol*. 1986:244(2):213–228.

Rajalingham R, Issa EB, Bashivan P, Kar K, Schmidt K, DiCarlo JJ. Large-scale, high-resolution comparison of the core visual object recognition behavior of humans, monkeys, and state-of-the-art deep artificial neural networks. *J Neurosci*. 2018:38(33):7255–7269.

Rauschecker JP. Where did language come from? Precursor mechanisms in nonhuman primates. *Curr Opin Behav Sci*. 2018:21:195–204.

Razi A, Seghier ML, Zhou Y, McColgan P, Zeidman P, Park HJ, Sporns O, Rees G, Friston KJ. Large-scale DCMs for resting-state fMRI. *Netw Neurosci*. 2017:1(3):222–241.

Rizzolatti G, Kalaska JF. Voluntary movement: the parietal and premotor cortex. In: Kandel ER, Schwartz JH, Jessell TM, Siegelbaum SA, Hudspeth AJ, editors. *Principles of neural science*. New York: McGraw-Hill; 2013. pp. 865–893

Rizzolatti G, Sinigaglia C. The mirror mechanism: a basic principle of brain function. *Nat Rev Neurosci*. 2016:17(12):757–765.

Rolls ET. Functions of the primate temporal lobe cortical visual areas in invariant visual object and face recognition. *Neuron*. 2000:27(2):205–218.

Rolls ET. Taste, olfactory, and food reward value processing in the brain. *Prog Neurobiol*. 2015:127-128:64–90.

Rolls ET. Functions of the anterior insula in taste, autonomic, and related functions. *Brain Cogn*. 2016a:110:4–19.

Rolls ET. *Cerebral cortex: principles of operation*. Oxford: Oxford University Press; 2016b.

Rolls ET. Reward systems in the brain and nutrition. *Annu Rev Nutr*. 2016c:36(1):435–470.

Rolls ET. Motivation explained: ultimate and proximate accounts of hunger and appetite. *Adv Motiv Sci*. 2016d:3:187–249.

Rolls ET. *The brain, emotion, and depression*. Oxford: Oxford University Press; 2018a.

Rolls ET. The storage and recall of memories in the hippocampo-cortical system. *Cell Tissue Res*. 2018b:373(3):577–604.

Rolls ET. *The orbitofrontal cortex*. Oxford: Oxford University Press; 2019a.

Rolls ET. The orbitofrontal cortex and emotion in health and disease, including depression. *Neuropsychologia*. 2019b:128:14–43.

Rolls ET. The texture and taste of food in the brain. *J Texture Stud*. 2020a:51(1):23–44.

Rolls ET. Spatial coordinate transforms linking the allocentric hippocampal and egocentric parietal primate brain systems for memory, action in space, and navigation. *Hippocampus*. 2020b:30(4):332–353.

Rolls ET. Neurons including hippocampal spatial view cells, and navigation in primates including humans. *Hippocampus*. 2021a:31(6):593–611.

Rolls ET. Mind causality: a computational neuroscience approach. *Front Comput Neurosci*. 2021b:15:70505.

Rolls ET. *Brain computations: what and how*. Oxford: Oxford University Press; 2021c

Rolls ET. Learning invariant object and spatial view representations in the brain using slow unsupervised learning. *Front Comput Neurosci*. 2021d:15:686239.

Rolls ET. Hippocampal spatial view cells for memory and navigation, and their underlying connectivity in humans. *Hippocampus*. 2022a. https://doi.org/10.1002/HIPO.23467.

Rolls ET. The hippocampus, ventromedial prefrontal cortex, and episodic and semantic memory. *Prog Neurobiol*. 2022b:217:102334.

Rolls ET, Deco G. Networks for memory, perception, and decision-making, and beyond to how the syntax for language might be implemented in the brain. *Brain Res*. 2015:1621:316–334.

Rolls ET, Treves A. The neuronal encoding of information in the brain. *Prog Neurobiol*. 2011:95(3):448–490.

Rolls ET, Scott TR, Sienkiewicz ZJ, Yaxley S. The responsiveness of neurones in the frontal opercular gustatory cortex of the macaque monkey is independent of hunger. *J Physiol*. 1988:397(1):1–12.

Rolls ET, Sienkiewicz ZJ, Yaxley S. Hunger modulates the responses to gustatory stimuli of single neurons in the caudolateral orbitofrontal cortex of the macaque monkey. *Eur J Neurosci*. 1989:1(1):53–60.

Rolls ET, Yaxley S, Sienkiewicz ZJ. Gustatory responses of single neurons in the caudolateral orbitofrontal cortex of the macaque monkey. *J Neurophysiol*. 1990:64(4):1055–1066.

Rolls ET, Critchley H, Wakeman EA, Mason R. Responses of neurons in the primate taste cortex to the glutamate ion and to inosine 5′-monophosphate. *Physiol Behav*. 1996:59(4–5):991–1000.

Rolls ET, O'Doherty J, Kringelbach ML, Francis S, Bowtell R, McGlone F. Representations of pleasant and painful touch in the human orbitofrontal and cingulate cortices. *Cereb Cortex*. 2003:13(3):308–317.

Rolls ET, Critchley HD, Verhagen JV, Kadohisa M. The representation of information about taste and odor in the orbitofrontal cortex. *Chemosens Percept*. 2010:3(1):16–33.

Rolls ET, Mills T, Norton A, Lazidis A, Norton IT. Neuronal encoding of fat using the coefficient of sliding friction in the cerebral cortex and amygdala. *Cereb Cortex*. 2018:28:4080–4089.

Rolls ET, Cheng W, Feng J. The orbitofrontal cortex: reward, emotion, and depression. *Brain Communications*. 2020:2(2):fcaa196.

Rolls ET, Deco G, Huang C-C, Feng J. Multiple cortical visual streams in humans. *Cereb Cortex*. 2022a. https://doi.org/10.1093/cercor/bhac276.

Rolls ET, Deco G, Huang C-C, Feng J. The human posterior parietal cortex: effective connectome, and its relation to function. *Cereb Cortex*. 2022b. https://doi.org/10.1093/cercor/bhac266.

Rolls ET, Deco G, Huang C-C, Feng J. Prefrontal and somatosensory-motor cortex effective connectivity in humans. *Cereb Cortex*. 2022c. https://doi.org/10.1093/cercor/bhac391.

Rolls ET, Deco G, Huang C-C, Feng J. The human language effective connectome. *NeuroImage*. 2022d:258:119352.

Rolls ET, Deco G, Huang CC, Feng J. The effective connectivity of the human hippocampal memory system. *Cereb Cortex*. 2022e:32:3706–3725.

Rolls ET, Deco G, Huang CC, Feng J. The human orbitofrontal cortex, vmPFC, and anterior cingulate cortex effective connectome: emotion, memory, and action. *Cereb Cortex*. 2022f. https://doi.org/10.1093/cercor/bhac070.

Rolls ET, Rauschecker JP, Deco G, Huang C-C, Feng J. Auditory cortical connectivity in humans. 2022g. Cerebral Cortex, in review.

Rolls ET, Wirth S, Deco G, Huang C-C, Feng J. The human posterior cingulate, retrosplenial and medial parietal cortex effective connectome, and implications for memory and navigation. *Hum Brain Mapp*. 2022h. https://doi.org/10.1002/HBM.26089.

Ronchi R, Park HD, Blanke O. Bodily self-consciousness and its disorders. *Handb Clin Neurol*. 2018:151:313–330.

Rozzi S, Calzavara R, Belmalih A, Borra E, Gregoriou GG, Matelli M, Luppino G. Cortical connections of the inferior parietal cortical convexity of the macaque monkey. *Cereb Cortex*. 2006:16(10): 1389–1417.

Salimi-Khorshidi G, Douaud G, Beckmann CF, Glasser MF, Griffanti L, Smith SM. Automatic denoising of functional MRI data: combining independent component analysis and hierarchical fusion of classifiers. *NeuroImage*. 2014:90:449–468.

Sallet J, Mars RB, Noonan MP, Neubert FX, Jbabdi S, O'Reilly JX, Filippini N, Thomas AG, Rushworth MF. The organization of dorsal frontal cortex in humans and macaques. *J Neurosci*. 2013:33(30): 12255–12274.

Satterthwaite TD, Elliott MA, Gerraty RT, Ruparel K, Loughead J, Calkins ME, Eickhoff SB, Hakonarson H, Gur RC, Gur RE, et al. An improved framework for confound regression and filtering for control of motion artifact in the preprocessing of resting-state functional connectivity data. *NeuroImage*. 2013:64:240–256.

Scheirer J, Ray WS, Hare N. The analysis of ranked data derived from completely randomized factorial designs. *Biometrics*. 1976:32(2): 429–434.

Scott TR, Yaxley S, Sienkiewicz ZJ, Rolls ET. Gustatory responses in the frontal opercular cortex of the alert cynomolgus monkey. *J Neurophysiol*. 1986:56(3):876–890.

Segerdahl AR, Mezue M, Okell TW, Farrar JT, Tracey I. The dorsal posterior insula subserves a fundamental role in human pain. *Nat Neurosci*. 2015:18(4):499–500.

Sinha N. 2022. *Non-parametric alternative of 2-way ANOVA (ScheirerRayHare) MATLAB central file exchange*: https://www.mathworks.com/matlabcentral/fileexchange/96399-non-parametric-alternative-of-96392-way-anova-scheirerrayhare.

Smith SM. Fast robust automated brain extraction. *Hum Brain Mapp*. 2002:17(3):143–155.

Smith SM, Beckmann CF, Andersson J, Auerbach EJ, Bijsterbosch J, Douaud G, Duff E, Feinberg DA, Griffanti L, Harms MP, et al. Resting-state fMRI in the human connectome project. *NeuroImage*. 2013:80:144–168.

Smith RE, Tournier JD, Calamante F, Connelly A. SIFT2: enabling dense quantitative assessment of brain white matter connectivity using streamlines tractography. *NeuroImage*. 2015:119:338–351.

Snyder LH, Grieve KL, Brotchie P, Andersen RA. Separate body- and world-referenced representations of visual space in parietal cortex. *Nature*. 1998:394(6696):887–891.

Sprung-Much T, Eichert N, Nolan E, Petrides M. Broca's area and the search for anatomical asymmetry: commentary and perspectives. *Brain Struct Funct*. 2022:227(2):441–449.

Squire LR. Memory and the hippocampus: a synthesis from findings with rats, monkeys and humans. *Psychol Rev*. 1992:99(2): 195–231.

Squire LR, Zola SM. Structure and function of declarative and nondeclarative memory systems. *Proc Natl Acad Sci U S A*. 1996:93(24): 13515–13522.

Sulpizio V, Galati G, Fattori P, Galletti C, Pitzalis S. A common neural substrate for processing scenes and egomotion-compatible visual motion. *Brain Struct Funct*. 2020:225(7):2091–2110.

Treves A, Rolls ET. A computational analysis of the role of the hippocampus in memory. *Hippocampus*. 1994:4(3):374–391.

Valdes-Sosa PA, Roebroeck A, Daunizeau J, Friston K. Effective connectivity: influence, causality and biophysical modeling. *NeuroImage*. 2011:58(2):339–361.

Van Essen DC, Glasser MF. Parcellating cerebral cortex: how invasive animal studies inform noninvasive mapmaking in humans. *Neuron*. 2018:99(4):640–663.

Van Essen DC, Smith SM, Barch DM, Behrens TE, Yacoub E, Ugurbil K, Consortium WU-MH. The WU-Minn human connectome project: an overview. *NeuroImage*. 2013:80:62–79.

Vedder LC, Miller AMP, Harrison MB, Smith DM. Retrosplenial cortical neurons encode navigational cues, trajectories and reward locations during goal directed navigation. *Cereb Cortex*. 2017:27(7): 3713–3723.

Verhagen JV, Rolls ET, Kadohisa M. Neurons in the primate orbitofrontal cortex respond to fat texture independently of viscosity. *J Neurophysiol*. 2003:90(3):1514–1525.

Verhagen JV, Kadohisa M, Rolls ET. The primate insular/opercular taste cortex: neuronal representations of the viscosity, fat texture, grittiness, temperature and taste of foods. *J Neurophysiol*. 2004:92(3):1685–1699.

Vogt BA. Midcingulate cortex: structure, connections, homologies, functions and diseases. *J Chem Neuroanat*. 2016:74:28–46.

Weiller C, Reisert M, Peto I, Hennig J, Makris N, Petrides M, Rijntjes M, Egger K. The ventral pathway of the human brain: a continuous association tract system. *NeuroImage*. 2021:234:117977.

Yaxley S, Rolls ET, Sienkiewicz ZJ. The responsiveness of neurons in the insular gustatory cortex of the macaque monkey is independent of hunger. *Physiol Behav*. 1988:42(3):223–229.

Yaxley S, Rolls ET, Sienkiewicz ZJ. Gustatory responses of single neurons in the insula of the macaque monkey. *J Neurophysiol*. 1990:63(4):689–700.

Yeterian EH, Pandya DN, Tomaiuolo F, Petrides M. The cortical connectivity of the prefrontal cortex in the monkey brain. *Cortex*. 2012:48(1):58–81.

Yokoyama C, Autio JA, Ikeda T, Sallet J, Mars RB, Van Essen DC, Glasser MF, Sadato N, Hayashi T. Comparative connectomics of the primate social brain. *NeuroImage*. 2021:245:118693.

Zhuang C, Yan S, Nayebi A, Schrimpf M, Frank MC, DiCarlo JJ, Yamins DLK. Unsupervised neural network models of the ventral visual stream. *Proc Natl Acad Sci U S A*. 2021:118(3):e2014196118.